BOREAL ENVIRONMENT RESEARCH 13: 475–502
ISSN 1239-6095 (print) ISSN 1797-2469 (online)
© 2008
Helsinki 30 December 2008

Momentum fluxes and wind gradients in the marine boundary layer — a multi-platform study

Ulf Högström[1)], Erik Sahlée[1)], William M. Drennan[2)], Kimmo K. Kahma[3)], Ann-Sofi Smedman[1)], Cecilia Johansson[1)], Heidi Pettersson[3)], Anna Rutgersson[1)], Laura Tuomi[3)], Fei Zhang[2)] and Milla Johansson[3)]

[1)] *Department of Earth Sciences, Meteorology, University of Uppsala, SE-752 36 Uppsala, Sweden*
[2)] *Rosenstiel School of Marine and Atmospheric Science, University of Miami, Miami, FL 33149-1098, USA*
[3)] *Finnish Institute of Marine Research, FI-00561 Helsinki, Finland*

Received 1 Aug. 2007, accepted 16 Jan. 2008 (Editor in charge of this article: Veli-Matti Kerminen)

Högström, U., Sahlée, E., Drennan, W. M., Kahma, K. K., Smedman, A.-S., Johansson, C., Pettersson, H., Rutgersson, A., Tuomi, L., Zhang, F. & Johansson, M. 2008: Momentum fluxes and wind gradients in the marine boundary layer — a multi-platform study. *Boreal Env. Res.* 13: 475–502.

During five autumn weeks, measurements of turbulent fluxes were obtained in the Baltic Sea at three levels on a 30-m tower and two levels on an ASIS buoy 4 km from the tower together with profiles of wind and temperature. Wave data and SST were obtained from ASIS. In the mean, momentum fluxes measured on the tower and on ASIS during onshore winds agree closely. Dimensionless wind gradients $\phi_m(z/L)$ for (i) stable conditions are linear in z/L (L is the Obukhov length); (ii) unstable, growing sea conditions are much smaller than predicted by 'standard' equations, due to an indirect effect of the boundary layer height. Individual wind profiles extrapolated from ASIS to tower by integration of $\phi_m(z/L)$ deviate by about 0.5 m s^{-1} from measured values, but corresponding mean profiles agree well for all levels from 1.18 m to 30 m. This random variation in the wind field is shown to be related to inherent dynamics of the atmospheric surface layer.

Introduction

In order to represent conditions over the open ocean, measurements of air–sea exchange should ideally be performed from platforms in deep water away from coastal influences. Such platforms can be ships or buoys. Problems related to contamination of the wind signals by platform motion were long troublesome, but with present technology in motion package systems, very reliable results can be obtained. Measurements onboard ships are usually plagued by complex, highly site-dependent flow-distortion effects, which can to some degree be corrected for by detailed physical or numerical flow modelling. With a specially designed ship and measuring masts these distortions can be greatly reduced provided that measurements are taken only when the ship motion is fairly small. Anchored buoys may offer ideal platforms with negligible flow distortion. Except for the case of the very sophisticated FLIP platform (FLIP: 'Floating Instrument Platform', *see* e.g. Schmitt *et al*. 1979, or Hristov *et al*. 2003), measurements from buoys are, however, restricted to one or maybe two levels in the lowest few meters above the water surface.

Another problem, which is common to all these measurements from sea-going platforms

is very strict restraint in time — measurement periods may last for weeks and possibly a few months but hardly more. In order to obtain air-sea interaction measurements from a site for periods of years, fixed installations are required. The ideal is, of course, a tower placed in deep enough water, such as the BIO (Bedford Institute of Oceanography) platform (Smith 1980), which was placed in 59-m-deep water in the Atlantic 10 km from the coast of Nova Scotia. The Dutch Meetpost Noordwijk, in 18 m of water in the North Sea, has produced many significant results (e.g. DeCosmo *et al*. 1996), but with some uncertainties at higher winds due to the limited depth (Oost 1998). Neither of these two towers had, however, profile measurements.

This paper will examine the characteristics of a particular station, the Östergarnsholm air–sea interaction station in the Baltic Sea. Data from this site have been used in a number of publications from the Uppsala group (e.g. Smedman *et al*. 1997, 1999, 2003, 2007). The crucial questions are in this case: do the measurements with a tower on land represent marine conditions? And further, do the measurements represent reasonably undisturbed upwind open ocean conditions? Theoretical considerations indicate that this is indeed the case, because most fluxes measured at an elevation above the ground represent a footprint (cf. Smedman *et al*. 1999) so far upwind that the land and shallow water effects near the measurement site do not necessarily influence them. If we study over water conditions it is sufficient that the footprints do not cover any land and that waves, currents and sea surface temperature are sufficiently homogenous in the footprint area. The requirements become more stringent if the measurements have to represent undisturbed open ocean conditions, because then the wave field has to represent undisturbed wave growth. In the present paper we have access to extensive data from an instrumented Air Sea Interaction Spar Buoy (ASIS) anchored in 36-m-deep water roughly 4 km in the upwind direction from the tower for a period of about 5 weeks as well as other dedicated measurements, as outlined in detail later. This enables a more direct test of how well the Östergarnsholm tower measurements represent the conditions of the upwind sea.

The measurements were part of a joint US–Swedish–Finnish project called BASE (BAltic Sea Swell Experiment). The main goal of the project was to combine experimental equipment available to the participating partners to study the swell regime in the Baltic Sea. Another goal was to use this instrumental setup to make the site evaluation outlined above. The present paper concentrates entirely on this subject and results of more general nature concerning the relations between momentum flux and wind gradients obtained in the analysis. The studies related to the swell regime are left for other, forthcoming publications.

Site, instrumentation and data selection

The experimental area is situated east of the island of Gotland in the Baltic Sea (Fig. 1). The instrumentation included the ASIS buoy supplied by the University of Miami, Miami, USA (RSMAS), the Östergarnsholm instrumented tower supplied by the University of Uppsala, Uppsala, Sweden (MIUU), and the r/v *Aranda*, two wave buoys and a current profiler supplied by the Finnish Institute of Marine Research (FIMR), Helsinki, Finland. In addition, a number of radio soundings were made by the Uppsala group at Östergarnsholm and by the Finnish group onboard r/v *Aranda*.

The Östergarnsholm tower and instrumentation

Östergarnsholm is a low island with virtually no trees (only a small group of trees around the lighthouse 1.5 km north of the tower, a sector not used here). The 1-km-long peninsula in the southern part of the island rises to no more than a couple of meters above mean sea level. A 30-m tower has been erected at the southernmost tip of this peninsula. The base of the tower is situated at about one meter above the mean sea level. As a result of meteorological forcing in the Baltic and surrounding seas (tide effects are of negligible magnitude), the actual sea level varied by about ±0.2 m during the BASE experiment. Sea level

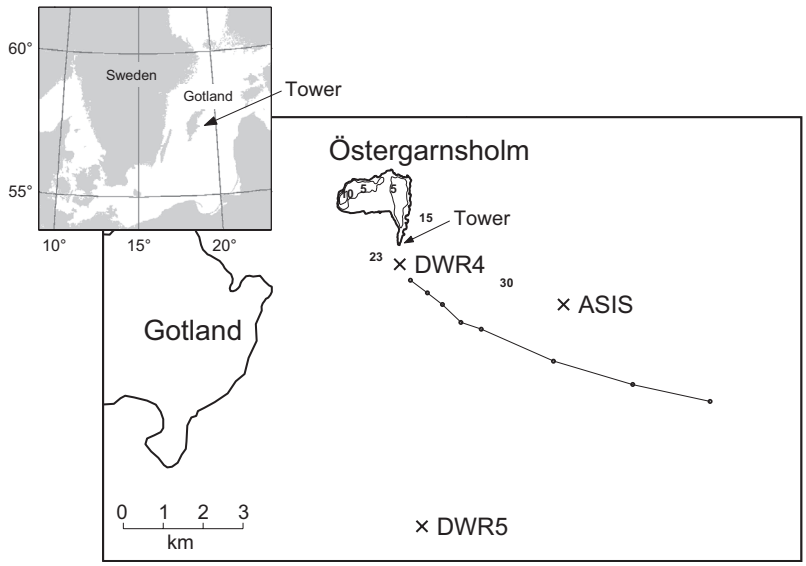

Fig. 1. Map of the BASE area. ASIS, DWR4 and DWR5 are measurement buoys. Anchor depths are 36 m, 15 m and 43 m, respectively. Also shown is a typical measurement track of r/v *Aranda* (10 Sep. 2003 at 02:13–12:27 UTC). with dots indicating measurement points. Height contours for 5 and 10 m are shown on the Östergarnsholm island. Numbers in boldface are water depths.

data valid also for the Östergarnsholm area are recorded at Visby harbour (data supplied by the Swedish Meteorological and Hydrological Institute) on the west coast of Gotland. The distance from the tower to the shoreline is only a few tens of meters in the sector with wind from NE to SW in the clockwise sense. The seafloor up to 500 m from the peninsula has an approximate slope of 1:30, varying somewhat in different directions. About 10 km from the peninsula, the depth is 50 m, reaching below 100 m farther out.

The 30-m tower was instrumented with Solent 1012 sonic anemometers (Gill Instruments, Lymington, UK) at 9, 16.5 and 25 m above the tower base. Turbulence data of temperature and the three wind components were recorded at 20 Hz. In addition, slow-response ("profile") sensors for temperature (copper-constantan thermocouples in ventilated radiation shields), wind speed and direction (light cup anemometers and wind vanes of in-house design) were recorded at 1 Hz at 6.9, 11.8, 14.3, 20.2 and 28.8 m. Humidity was recorded at 9 m with a LICOR LI-7500 (for the rapid fluctuations) and at 7 m with a Rotronic (Young Co.) instrument (for the slow variations). The mean height of the tower base above the sea level was 1.3 m, with a range of ±0.2 m. In the text we use the nominal mean heights above sea level: 10, 18 and 26 m for the turbulence instruments; 8.1, 13.1, 15.5, 21.5 and 30.0 m for the profile instruments.

The sonic and the cup anemometers were calibrated in a large wind tunnel prior to the experiment. The sonic temperature is corrected for cross wind effects following Kaimal and Gaynor (1991). In order to remove possible trends, a high-pass filter based on a 10-minute linear detrending was applied to the turbulence time series prior to calculating moments (variances and co-variances). Both turbulence and 'profile' data are 30 min averages compiled using three consecutive 10-minute periods.

The ASIS buoy

The ASIS (Fig. 2) is a multi-spar buoy, which can be described as a pentagonal cage of slender cylinders (Graber *et al*. 2000). The side of the pentagon is 1.6 m; the cylinders have a diameter of 0.2 m and a length of 3.5 m. Attached to the bottom of the "cage" is a 4-m-long centrally-located cylinder ending with a drag plate on which the heavy batteries needed for power supply are placed together with the motion package (*see* below) and data logger. Most of the spar buoy was immersed in water with only the uppermost ca. 100 cm of the cylinders extending above the water level (Fig. 2). On top of the 'cage' there is an open platform, which is the base for a 4.5-m high slender open lattice mast of triangular cross section of ca. 0.15-m side. On

Fig. 2. The ASIS buoy (in the foreground) with r/v *Aranda* in the background.

the cage platform there is also some recording equipment. To avoid downward forces generated by a subsurface anchor, the buoy is attached with a 60-m-long surface tether to a separate mooring buoy.

The buoy operated from 3 September to 10 October, and again from 24 to 27 October 2003 after the batteries were replaced. For future reference, these two periods will be referred to as D1 and D2, respectively.

ASIS was equipped as follows: two Gill R2A sonic anemometers at 5.3 and 2.56 m above mean water level (MWL) measured the three components of wind speed and sonic temperature. A third sonic at 4.0 m failed. The anemometers were calibrated at Gill prior to the deployment. The 2.5 m sonic was "zeroed" in the field by sticking a foam-insulated bucket over the sonic head and leaving it there for several minutes with the data acquisition system running. Air temperature and humidity were measured using a shielded Vaisala HMP 45 sensor at 4.3 m. An array of 3.3 m long 9.10^{-4} m diameter capacitance wave gauges, arranged in a 0.93 m radius centered pentagon measured surface elevation. The wave staffs were calibrated in a large tank in Helsinki prior to the deployment. All the above heights refer to D1. For D2, all heights should be increased by 0.3 m.

Both the sonic anemometers and wave gauges were corrected for the motion of ASIS, which was measured using redundant motion packages in watertight housings 7.7 m below the water. Each motion package consists of 3 orthogonally mounted Columbia Research Laboratory SA-307HPTX linear accelerometers, 3 orthogonally mounted Systron Donner CG1-00050-100 rate gyros and a Precision Navigation TCM-2 compass. The above data were all sampled at 20 Hz, and analyzed in 30-minute files. Processing of the anemometer data followed the tower procedures. In addition, the data for the wind direction from behind the sonic (i.e. through the struts of the sensor head) were rejected. This primarily affected low wind (< 3 m s^{-1}) cases, as ASIS tends to point into the wind for higher winds.

Mean wind speed and direction were measured using Vaisala WM301 cup anemometers and vanes at 2.42 and 1.18 m. Air temperature was measured at 1.7 and 0.7 m above MWL using aspirated copper-constantan thermocouples. These, along with the Vaisala anemometers were mounted on 0.6-m-long booms pointing towards the port side of ASIS. The thermocouples and Young anemometers were sampled every 10 s by a Campbell recorder located on the ASIS deck. They operated only during D1. The positioning of the lowest thermocouple only 0.70 m above MWL and cup anemometer at 1.2 m was thought feasible due to ASIS' property of following the longer waves (Graber *et al*. 2000). Although it only provided three days of clean data before being hit by a wave, these data are unique in their proximity to the water. Note that, as seen in Fig. 2, the cup anemometer at 1.2 m above MWL was attached (with a 0.6-m-long boom) to one of the 0.2 m diameter cylindrical legs of the buoy, which means that special care must be taken to identify and quantify possible flow distortion effects (*see* below).

Sea surface temperature was measured by an array of six self-logging thermistors (5 Hugrun Seamon UTR-100, and 1 Brancker TR-1000F) mounted on ASIS between 1 and 8 m below MWL. The thermistors were calibrated at Miami before and after the experiment. An upward-looking 300 kHz ADCP was moored nearby ASIS, measuring current profiles every 2 m through the water column.

Wave data are analyzed following Pettersson *et al*. (2003). The parameters of particular interest here are the significant wave height H_s, calculated as four times the standard deviation of surface elevation and peak frequency f_p. In addition, the wave array data are processed using a maximum likelihood method algorithm to yield directional spectra. These spectra are analyzed using a wave partitioning algorithm (Gerling 1992) to yield the individual wave systems, either wind seas or swell. For each of the systems, the energy, peak frequency and peak propagation direction ϕ_d are calculated. Here we define as wind sea a wave train travelling within ±40° of the wind direction ϕ, and which meet the wave age criterion $U_{10N}\cos(\phi - \phi_d) > 0.83c_p$ (Donelan *et al*. 1985), where c_p is the peak wave phase velocity (calculated from f_p), and U_{10N} is the neutral wind speed at 10 m.

Directional wave buoys

Directional wave parameters were also calculated from two Datawell Directional Waverider (DWR) buoys moored at 57°25.55´N, 18°59.25´E in 15-m deep water, DWR4 (Fig. 1), and at 57°22´N 18°59.5´E, in 43-m-deep water, DWR5. The buoys were operational from 3 September to 27 October. A comparison of data from the three buoys (DWR and ASIS) allowed for the investigation of the homogeneity of the wave field in the vicinity of ASIS and the Östergarnsholm tower (*see* below). A previous side-by-side comparison of ASIS and DWR showed good agreement (Pettersson *et al*. 2003).

Aranda measurements

Aranda (Fig. 2) made two cruises during the experiment, one in the beginning and one in the end of the experiment, and the total measurement period was approximately seven days. The turbulence measurements on board were made at the bow mast of the ship at the height of 16 m. Since a helicopter landing platform is situated at the bow deck of the ship, there are no massive structures causing severe flow distortions at the bow. The distance between the bow mast and the edge of the bow is 1.2 m. A sonic anemometer (Metek USA-1) and a LICOR LI-7500 CO_2/H_2O open path analyzer were mounted at the top of the mast on a stand designed for minimum flow distortion. A motion sensor (Kongsberg Seatex MRU-6) was mounted 1.6 m below these sensors. The bow of the ship was also equipped with a Miros microwave radar for measurement of the waves. The ship's weather station, which is situated in the middle part of the ship, provided the basic meteorological information. The sea surface temperature is measured at a depth of 4 m with a sensor attached to the bulk of the ship. The weather information, position, heading and speed of the ship was recorded once in a minute.

During the measurements, the bow of the ship was kept within ±20 degrees in the wind direction. Measurements were made close to the tower and the ASIS buoy as well as along several horizontal profiles originating from the tower. During these profiles the ship stayed at one position for half an hour and moved during the following half-hour in the wind direction at a speed of 0.5–1 knots (Fig. 1). The sampling frequency for the sonic anemometer was 10 Hz and for the motion sensor 2 Hz. Like in the case of the ASIS buoy, the six components of motion from the motion sensor were used to correct the sonic anemometer time series. The correction was made following the method of Drennan *et al*. (1994).

Weather and footprint analysis

Meteorological conditions during BASE

The general weather regime in the BASE area during the measurement campaign (3 September to 27 October 2003) was that of high cyclonic activity. Thus, low pressure disturbances were

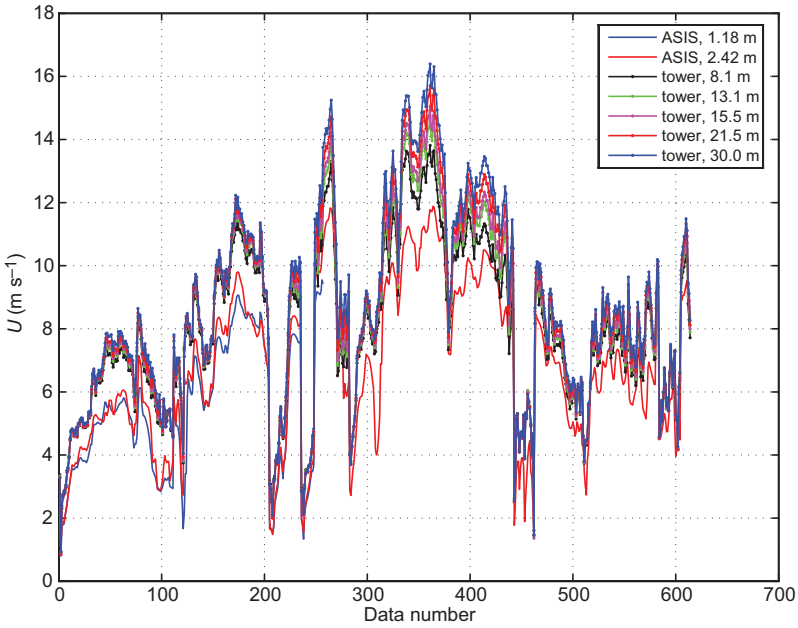

Fig. 3. Wind speed (m s^{-1}) measured by cup anemometers at ASIS (two levels) and on the tower (5 levels) plotted against data number for the basic data set.

passing in rapid succession along the west to east or southwest to northeast track, with brief periods in between characterized by a high pressure ridge extending northward over Sweden from a vast high pressure system with its central parts residing over northern continental Europe during most of the time period. This weather regime led to strong variability in wind speed and direction in the experimental area (Figs. 3 and 4). The sea surface temperature measured from ASIS was about 16.5 °C at the onset but dropped to below 13 °C at end of the experiment (Fig. 5). Two periods with rapid decrease in water temperature are marked. As discussed later, detailed analysis shows that these periods were characterized by strong upwelling. From the course of the 10-m air temperature it is clear that periods with air colder than the water occurred during some parts of the time — giving rise to unstable atmospheric stratification — and periods with air warmer than the water during other parts — resulting in stable atmospheric stratification. A measure of the degree of stratification is given by the Obukhov length

$$L = -\frac{u_*^3 T_0}{gk\overline{w'\theta_v'}} \qquad (1)$$

where

$$u_* = \sqrt{-\overline{u'w'}}$$

is the friction velocity (m s^{-1}), T_0 is the mean temperature of the atmospheric surface layer in Kelvin, g is acceleration of gravity (m s^{-2}), k is the von Karman constant (= 0.4) and $\overline{w'\theta_v'}$ is the vertical flux of virtual potential temperature (m s^{-1} K).

As discussed in detail later, the basic data set contains 178 data with stable stratification, i.e. positive L, and 572 values with unstable stratification, i.e. negative L values. Statistical analysis of the distribution of L values shows that $L > 100$ m during 92% of the time with stable stratification; for unstable conditions, $-L$ values > 100 m occur during about 60% of the time. These distributions show that a combination of low heat flux and high wind (i.e. high u_*) prevailed during most of the time. Corresponding statistics for what is termed the "profile" data set (*see* below) agrees very well with that of the basic data set.

Footprint calculations for BASE

The flux of some quantity measured at a height z above the water surface can be considered

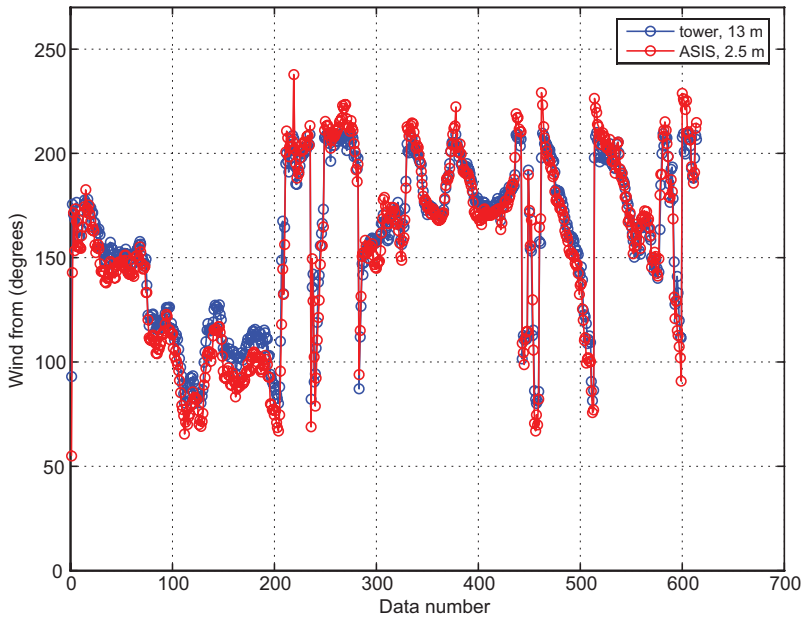

Fig. 4. Wind direction at ASIS, 2.5 m and on the tower at 13 m plotted against data number.

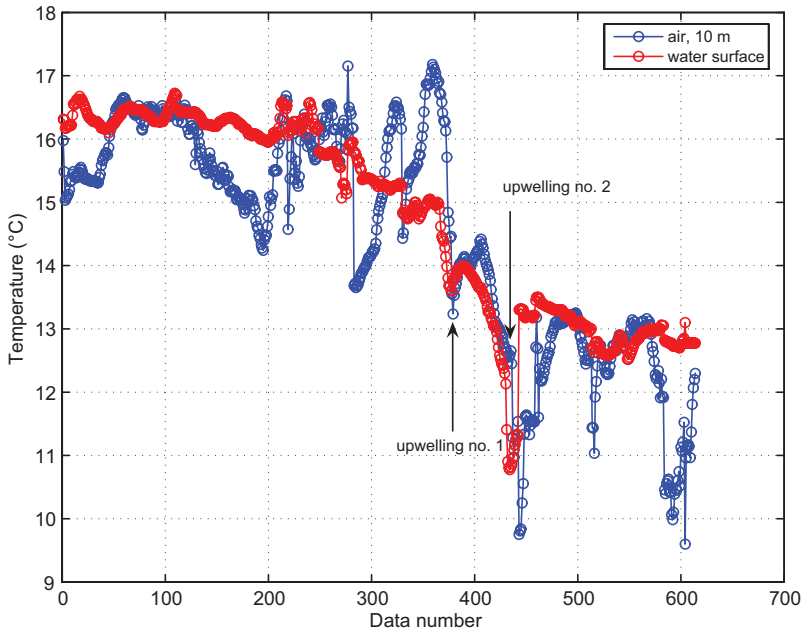

Fig. 5. Air temperature at 10 m on the tower and water surface temperature from ASIS plotted as function of data number. Also indicated is onset time for two situations with upwelling.

the integral of contributions to surface fluxes of this quantity from a row of infinitely wide line sources oriented perpendicular to the mean wind direction during each particular 30 minute run. As shown by Smedman *et al*. (1999: appendix A), it is possible to apply expressions originally developed for calculation of atmospheric dispersion of air pollutants to make quantitative estimates of the relative role of upwind areas at different distances in the total measured flux. These calculations are considered reliable, as they are based on a set of mathematical expressions which are theoretically well founded and which have been validated against data from controlled field experiments of atmospheric dispersion of inert tracers.

For the BASE experiment, flux footprint estimates are needed not only for the heights of the turbulence instruments on the Östergarnsholm tower — 10, 18 and 26 m (which were given by Smedman *et al*. 1999), but also for the corresponding heights of the turbulence instruments on the ASIS — 2.5 and 5 m. As the flux footprint is highly dependent on atmospheric stability, calculations have been carried out for five values of Obukhov's length L (Eq. 1): two unstable cases, L = –10 m and –100 m; ±∞ = neutral; two stable cases, L = +100 m and +10 m for each measuring height.

Footprint calculations have been made (Table 1) for the heights 2.5, 10, 18 and 26 m for the five stability categories. The last column gives an indication of the areal extent of the footprint. It has been derived on the following premises: From dispersion theory (*see* e.g. Pasquill and Smith 1983) it can be inferred that the lateral extension of the flux footprint is expected to have an approximate Gaussian distribution at each distance from the measuring point. The standard deviation of this distribution σ_y (m) is expected to increase linearly with distance and be related to the corresponding standard deviation of the lateral component of the wind, σ_v (m s^{-1}):

$$\sigma_y = (\sigma_v/U_z)x = \sigma_\phi x \qquad (2)$$

where U_z is the mean wind speed (for the particular 30 minute period) at the measuring height z. We define arbitrarily a "width" of the flux footprint at any distance x as $4\sigma_y$, which means that we include 95% of the flux contribution laterally. This defines a footprint area in the shape of an isosceles triangle with the apex at the measurement point, extending in the mean wind direction. If we further restrict the footprint to $x_{20\%} < x < x_{80\%}$ (Table 1), the corresponding area becomes

$$A = 2\sigma_\phi \left(x_{80\%}^2 - x_{20\%}^2\right) \qquad (3)$$

The most stable case, L = 10 m gives footprints (Table 1) that extend to far greater distances than any of the other cases, but as noted above, such cases occur so seldom that they

Table 1. Flux footprint (z) calculations for measuring heights 2.5, 10, 18 and 26 m for five stability categories. 20%–80% area (m^2) = area for the flux contributions 20%–80% based on criteria for 95% lateral extension as explained in the text.

		Distances for cumulative flux fractions			
z (m)	Stability category	$x_{50\%}$ (m)	$x_{20\%}$ (m)	$x_{80\%}$ (m)	20%–80% area (m^2)
2.5	neutral	140	80	320	1.4×10^4
2.5	L = –100 m	110	65	250	8.7×10^3
2.5	L = –10 m	80	45	140	2.6×10^3
2.5	L = 100 m	160	125	900	1.2×10^5
2.5	L = 10 m	900	180	5500	4.5×10^6
10	neutral	600	300	1500	3.2×10^5
10	L = –100 m	275	175	800	9.1×10^4
10	L = –10 m	150	75	300	1.3×10^4
10	L = 100 m	1400	400	6500	6.3×10^6
10	L = 10 m	6000	1700	22000	7.2×10^7
18	neutral	1200	600	3000	1.3×10^6
18	L = –100 m	600	300	1100	1.7×10^5
18	L = –10 m	250	250	500	2.8×10^4
18	L = 100 m	3500	1500	15000	3.3×10^7
18	L = 10 m	13000	3300	51000	3.9×10^8
26	neutral	1700	900	5000	3.6×10^6
26	L = –100 m	850	500	1900	5.0×10^5
26	L = –10 m	350	225	600	4.6×10^4
26	L = 100 m	6200	1700	30000	1.3×10^8
26	L = 10 m	29000	6000	120000	2.2×10^9

can be disregarded as not representative of the present data set. But the most unstable case, L = –10 m is also fairly uncommon, so the remaining three stability cases give a reasonably consistent picture which can then be considered as representative for the experimental conditions during most of the time in BASE. Thus, a mean $x_{50\%}$ value can be derived based on the three cases of neutral, L = –100 m and L = +100 m for each measuring height, giving $x_{50\%}$ = 140 m for z = 2.5 m, 760 m for z =10 m, 1800 m for z = 18 m and 2900 m for z = 26 m. The corresponding mean $x_{80\%}$ values are: 490 m for z = 2.5 m, 2900 m for z = 10 m, 6400 m for z = 18 m and 12 000 m for 26 m respectively. Corresponding geometrical mean footprint areas (Table 1, last column) are: 24 000 m^2 for z = 2.5 m, 570 000 m^2 for z = 10 m, 1 900 000 m^2 for z = 18 m and 6 200 000 m^2 for z = 26 m. These large differences in representative footprint distances and areas for the various measuring heights must be kept in mind when comparing the data from this experiment.

Wave field analysis and data selection

Wave field analysis

The study of the wave field focused on the three 1-D parameters, H_s, f_p and peak wave direction, as well as on the characteristics of individual wave trains or systems as measured by the three wave sensors (Fig. 1). As the particular emphasis of this paper is on growing seas, we focus on the wind sea component, those shorter waves travelling within 45° of the wind, with $c_p/U_{10} < 1.2$.

Based on the flux footprint analysis, wind directions from 50° through south to 210° yield marine conditions at the tower. For winds from 210°–220°, data in unstable flow represent marine conditions, while during stable conditions a portion of the footprint of the upper mast may be over land (depending on the magnitude of L), a minor peninsula being situated at x = 25 km and 220°. $x_{80\%} < 30$ km for $L > 100$ m. As with any coastal site, we must also distinguish between conditions truly representative of the open ocean *versus* those influenced to some degree by either the surrounding shorelines, which tend to produce directionally skewed wave fields, or shallow bathymetry, which affects the wave field through refraction and shoaling. In the case of the tower, two sectors are potentially influenced by these conditions. We discuss each separately.

Some 2–3 km NNE of the tower site lies a shoal of some 6–15 m depth. While the shoal is largely transparent to shorter wind sea waves (frequencies above 0.3 Hz), it effectively refracts longer waves coming from 50°–80°. The size of the sector affected by the shoal was studied with a refraction model of FIMR and also with WAM wave model (Komen *et al*. 1994) runs during the time period of the experiment. The changes in the wave field caused by the shoal were also clearly seen in the BASE data campaign on 28 September (not one of the days selected for flux analysis). On this day, a 0.5-m swell of 0.16 s (60 m wavelength) from NE was dominant at both ASIS and DWR5 (which were not in the lee of the shoal), but absent from DWR4 (in the lee of the shoal). Hence the 50°–80° sector represents open ocean conditions only in the absence of swell and when the frequency of the waves is above 0.33 Hz and above 0.25 Hz, respectively. The wind sea conditions studied here fulfil this requirement.

For winds and waves from 90°–190°, the tower effectively sees open ocean conditions: the tower footprint is entirely over water, and the waves are unaffected by direct coastal effects. An analysis of the wave field properties shows no significant differences between the three buoys (not shown).

For winds from 200°–210°, the tower data are representative of coastal marine conditions. Here the proximity of the land (Gotland Island) extending roughly SW (220°) from the tower strongly restricts the development of waves propagating from the land, resulting in a skewed directional energy distribution. This can be clearly seen in the directional wave data (Fig. 6). For winds from 200°–210° (Fig. 6b), the mean spectral peak of the wind sea waves at the near shore buoy DWR4 is skewed ten degrees away from the wind direction. In contrast the mean spectral wind sea peaks at the other two buoys further offshore are aligned with the wind. In case of the mean wind sea peak directions for winds from the sector 210°–220°, the wave fields

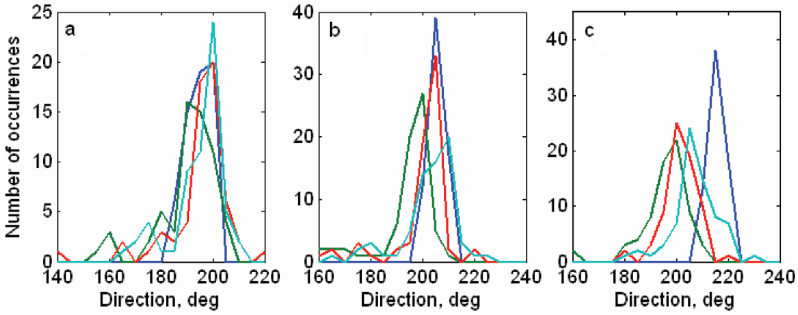

Fig. 6. Peak wind sea wave directions from ASIS (cyan), DWR5 (red) and DWR4 (green) for wind directions between (**a**) 185°–200°, (**b**) 200°–210°, and (**c**) 210°–220°. The wind direction distribution in each subplot is given by the blue curve.

at all three buoys are clearly skewed by shoreline effects (Fig. 6c).

Data selection

All the data from the Östergarnsholm tower, the ASIS buoy and the directional waveriders were put together in a common data base, which consists of successive 30-minute data and is fully synchronized in time. In all, it consists of 2722 half-hour data which each contain 411 parameters. The Östergarnsholm data are, however, meaningful only when the wind comes from directions with long (> 100 km) unobstructed over-water fetch. In previous papers, the Uppsala group has used the following criterion for the wind direction: $80° < \phi < 220°$. As noted above, the wave field is disturbed for winds in the sector 210°–220°. Thus including only data that fulfil the criterion $80° < \phi < 210°$ and removing data when ASIS was not operating, leaves a data set with 750 half-hour values, which will be denoted "the basic data set". Some additional analyses will be performed for the sector $210° < \phi < 220°$.

As noted above, provided the wind is strong enough, the ASIS buoy tends to turn downwind. The two R2A-sonics are mounted in such a way that they will then ideally get the wind centrally into the open 240° sector of the instrument. The sonic wind measured at 2.56 m can be compared with independent cup anemometer measurements at 2.42 m (Fig. 7). For $|\delta\phi_r| < 30°$ there is some scatter, but the mean is very close to zero. For $\delta\phi_r < -30°$, the cup is blocked to some extent by the sonic, resulting in increased scatter and a mean difference of 0.5 m s^{-1} or more. Because of this result, a data subset has been defined which satisfies the criterion $|\delta\phi_r| < 30°$, which we call the "profile data set", this term referring to the fact that (as outlined below) the wind profile analysis is particularly sensitive to the accuracy of the wind measurements. It contains 236 half-hour data. All statistical tests will be carried out both on the "basic data set" and on the "profile data set". Wind profile tests are based exclusively on the "profile data set".

Results

Comparison of turbulent fluxes of momentum from ASIS and the tower

The friction velocity u_* is defined as

$$\tau_0 = -\rho\left(\overline{u'w'}\right)_{z=0} = \rho u_*^2 \qquad (4)$$

where ρ is density of the air and $-\left(\overline{u'w'}\right)_{z=0}$ is the shearing stress at the surface. This expression defines u_* in the strict sense. In stationary and horizontally uniform conditions, $-\overline{u'w'}$ is expected to decrease slowly with height. In fact, an often used definition of the depth of the surface layer allows for a ten percent decrease of the shearing stress $\tau(z)$ from its surface value. Below, we will compare estimates of "friction velocity" in a "local" sense, which allows comparisons of measurements at various heights at the Östergarnsholm tower and ASIS:

$$u_*(z) = \sqrt{\tau(z)/\rho} = \sqrt{-\overline{u'w'}(z)} \qquad (5)$$

From a time plot (Fig. 8) for the basic data set of u_* measured at the levels 2.56 m and 5.3 m at ASIS and 10, 18 and 26 m on the Östergarnsholm tower it is clear that the data follow each other closely in general.

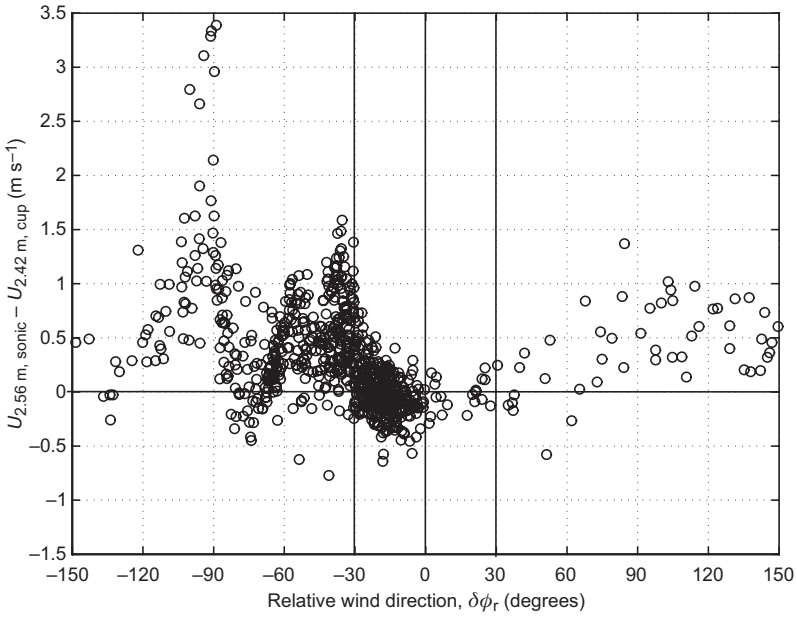

Fig. 7. The difference between wind speed at 2.56 m (sonic) and 2.42 m (cup anemometer) plotted against relative wind direction $\delta\phi_r$, i.e. the angle between actual wind and orientation of the symmetry axis of the sonic. Basic data set.

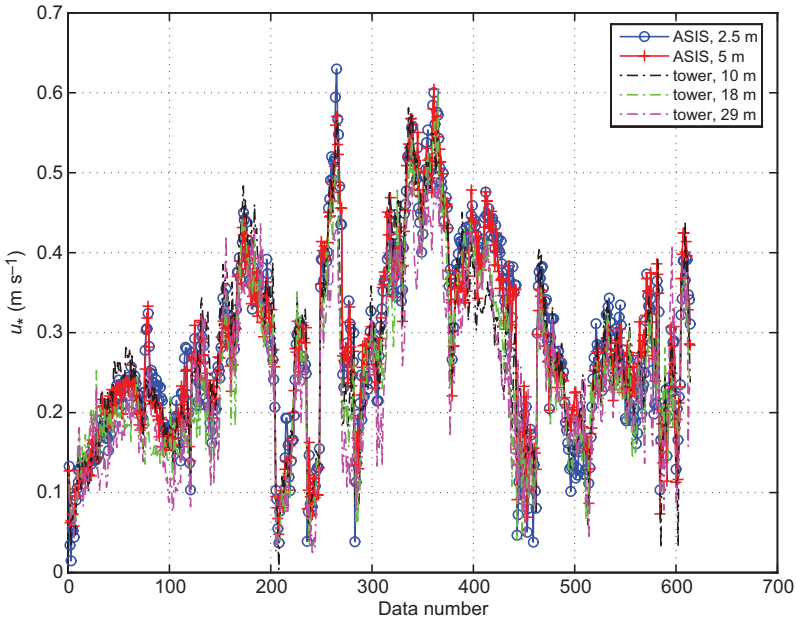

Fig. 8. "Local" friction velocity u_* for two levels on ASIS and three levels on the tower plotted against data number.

A statistical overview of the same data (Table 2) in terms of mean ratios of $u_*(z)/u_*(2.5\ m)$, where z takes the values 5, 10, 18 and 26 m, respectively, and corresponding standard deviations enables the following conclusions:

1. There is no systematic difference of the mean ratios between the basic case and the "profile" data.
2. The mean u_* ratios up to 10 m are close to unity for all cases; for stable conditions, however, a systematic reduction of 6%–9% is observed at 10 m, cf. below.
3. Above 10 m a slow systematic decrease of the mean u_* ratios is observed for all categories; for growing sea and mixed seas this systematic decrease appears first at 18 m, but for stable conditions it starts at 10 m.

Table 2. u_* ratios (± SD).

wind direction →	All cases		Growing sea		Mixed seas		Stable conditions		Unstable conditions	
	$80° < \phi < 210°$		$80° < \phi < 210°$		$80° < \phi < 210°$				$220° > \phi > 210°$	
wave age →	all		$c_p/U_{10} < 0.8$		$1.2 > c_p/U_{10} > 0.8$				$c_p/U_{10} < 1.2$	
	Basic data set	Profile data set	Basic data set	Profile data set	Basic data set	Profile data set	Basic data set	Profile data set	Basic data set	Profile data set
$u_{*5}/u_{*2.5}$	1.05 ± 0.26	1.00 ± 0.25	1.00 ± 0.10	0.97 ± 0.10	1.01 ± 0.14	0.98 ± 0.09	1.02 ± 0.13	1.00 ± 0.07	1.03 ± 0.22	1.02 ± 0.13
$u_{*10}/u_{*2.5}$	1.03 ± 0.33	1.00 ± 0.19	0.99 ± 0.13	1.04 ± 0.11	1.06 ± 0.21	1.07 ± 0.20	0.93 ± 0.15	0.91 ± 0.16	0.92 ± 0.15	0.94 ± 0.13
$u_{*18}/u_{*2.5}$	0.94 ± 0.38	0.95 ± 0.30	0.93 ± 0.17	0.96 ± 0.15	0.92 ± 0.19	0.87 ± 0.13	0.88 ± 0.14	0.89 ± 0.10	0.96 ± 0.21	0.95 ± 0.17
$u_{*26}/u_{*2.5}$	0.91 ± 0.41	0.90 ± 0.33	0.87 ± 0.17	0.90 ± 0.16	0.90 ± 0.29	0.92 ± 0.18	0.82 ± 0.19	0.84 ± 0.15	0.82 ± 0.18	0.85 ± 0.15
Mean 10 m wind speed (m s^{-1})	7.88	8.80	8.45	9.23	7.94	8.25	10.09	10.20	7.39	8.25
Number of data	750	236	125	86	122	37	178	79	97	46

4. The standard deviation of the u_* ratios is 0.3 in the mean when all cases and heights are taken together but only 0.14 for the growing sea case, 0.18 for mixed seas and 0.14 for the stable case.
5. For 'the coastal sector, $220° > \phi > 210°$, the ratio remains also close to unity up to 18 m, decreasing to similar values at 26 m as for the "basic" case. The standard deviation is 0.17 in the mean. Thus, no effect from the distorted wave field in this sector can be seen in the u_*-ratio statistics for the unstable cases.
6. Most importantly, it can be concluded that, in the mean, the momentum flux measured at 2.5 and 5 m at ASIS matches very well the corresponding flux measured at 10 m on the Östergarnsholm tower, the ratio $u_*(z)/u_*(2.5$ m) decreasing to about 0.88 at 26 m, which is of the expected magnitude from Rossby number similarity (cf. e.g. Stull 1988: chapter 9.8) considering typical u_* values and cross-isobaric angles for the present situation.

Turbulent fluxes of momentum from r/v *Aranda*

Friction velocity measurements made from r/v *Aranda* at a height of 16 m and at a distance of 200–300 m from ASIS and within 4 km of the tower were compared with corresponding data from ASIS (Fig. 9a) and the tower (Fig. 9b). The wind direction measured at the tower was between 80°–130°. The agreement between the ship-borne measurements and the corresponding ASIS and tower measurements is quite satisfactory.

In all, 10 horizontal measurement tracks from and towards the tower were performed with r/v *Aranda* when the wind direction was suitable. The first six (P1–P6) of these contain complete information from all three platforms and have been used here (Table 3). As an example *Aranda* results from one of the cruises (P3) are also plotted as a function of distance (Fig. 10). This particular track is displayed in the map of the area (Fig. 1). The time variation was removed from the horizontal *Aranda* profiles using Taylor's hypothesis. In case of wind speed the equation was

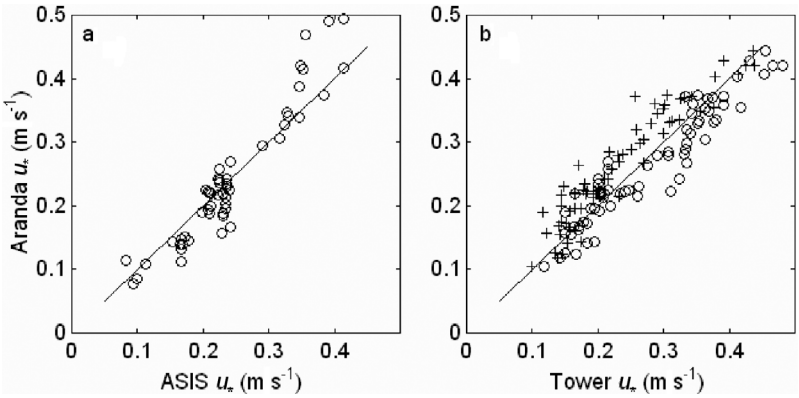

Fig. 9. — **a**: The friction velocity (u_*) measured on r/v *Aranda* at the height of 16 m plotted against the friction velocity from ASIS (5.3 m). The distance between r/v *Aranda* and ASIS was about 200–300 metres. — **b**: u_* from r/v *Aranda* compared with the u_* from the tower when the ship was less than 4 km from the tower. Circles = tower measurements at the height of 10 m; crosses = tower measurements at the height of 18 metres; solid line = 1:1 fit.

$$U_{Ac}(t) = U_A(t) - U_t(t + X/U_t) + \text{mean}(U_t)$$

where $U_A(t)$ is the wind speed measured at *Aranda* at time t and $U_{Ac}(t)$ the time variation of the corrected wind speed at time t, U_t is the wind speed at the tower and X/U_t is the time it takes the fluctuations to travel from *Aranda* the distance X to the tower. The general agreement between the measurements from the three platforms is quite good, the mean differences of u_* all being in the range 0–0.06 m s^{-1}. The profiles where the time variation has been removed are flat without any trend. Thus the 38 hours of measurements with r/v *Aranda* cruising in the range 0 to about 8 km from Östergarnsholm strongly support the results presented in the previous sub-section, concerning the horizontal homogeneity in the mean of the meteorological fields (more precisely of u_*).

The flux of sensible heat

A time plot of the temperature flux $\overline{w'\theta_v'}$ (Fig. 11) at 2.5, 5, 10, 18 and 26 m for the basic data set shows that, in general, the measured fluxes follow each other reasonably well, but with relative differences considerably larger than in the corresponding plot for the momentum flux, (Fig. 8). This is, however, understandable, as the magnitude of the heat flux is often close to the expected noise level. A flux ratio analysis similar to that shown for the momentum flux (Table 2) has been carried out for the heat flux as well (not shown). The general result is similar to that of the momentum flux, but the scatter is much larger, as might be expected in view of the smallness of the heat flux magnitude, $|\overline{w'\theta_v'}|$ being < 0.02 m s^{-1} K during a considerable part of time.

Table 3. Friction velocity comparison from horizontal profiles. Mean wind speed and direction is given as background information (5.3 m on the ASIS and 10 m on the tower and *Aranda*). All profiles started near the tower and passed ASIS. Profile P3 discussed in the paper is included in Fig. 1.

Profile & start time	Measurement duration (hours)	Length (km)	Mean wind (m s^{-1})	Mean wind dir. (°)	u_* ± SD (m s^{-1})		
					Aranda, 16 m	Tower, 18 m	ASIS, 5 m
P1 8 Sep. 2003, 10:55	4.1	1.6	4.7	96	0.15 ± 0.02	0.15 ± 0.01	0.19 ± 0.01
P2 8 Sep. 2003, 22:46	3.6	3.6	5.1	87	0.17 ± 0.05	0.16 ± 0.02	0.20 ± 0.04
P3 10 Sep. 2003, 2:13	10.2	8.3	8.3	104	0.30 ± 0.06	0.24 ± 0.06	0.28 ± 0.03
P4 10 Sep. 2003, 14:05	11.3	8.4	10.3	105	0.38 ± 0.04	0.37 ± 0.06	0.38 ± 0.04
P5 11 Sep. 2003, 2:59	4.6	2.6	9.7	100	0.35 ± 0.02	0.32 ± 0.03	0.35 ± 0.03
P6 11 Sep. 2003, 8:41	4.6	2.2	8.2	81	0.28 ± 0.03	0.25 ± 0.02	0.29 ± 0.03

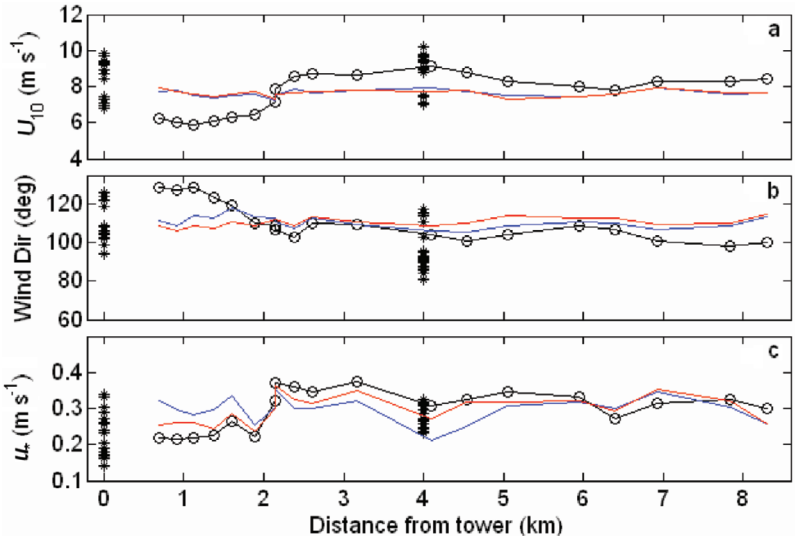

Fig. 10. Horizontal profiles from r/v *Aranda* measured on 10 Sep. 2003 at 02:13–12:27 UTC (black lines with circles). Red curves = tower measurements at 16 and 18 m corrected using Taylor's hypothesis; blue curves = ASIS data corrected using Taylor's hypothesis. — **a**: wind speed at 10 m; — **b**: wind direction; — **c**: friction velocity. Stars at the distance 0 km are half-hour tower data during the 10-hour measuring period; stars at 4 km are corresponding ASIS data. The ship track is plotted in Fig. 1.

During situations with upwelling (indicated with arrows in Fig. 11), the surface temperature field varied considerably both in space and time. In view of the results from the footprint analysis (Table 1), it would be expected that the turbulence instruments at the different levels on the tower and ASIS may have measured different heat fluxes. That this is indeed so, is vividly illustrated in the insert in Fig. 11, which shows the sensible heat flux during part of the time during the first upwelling period, 22–23 Sep. 2003. Thus, as a result of the surface temperature patchiness during the first ca. 30 half-hours, the flux at 18 and 26 m was only about half of that measured at a lower height.

Wind profile analysis

Special study of the ASIS wind profile

As explained previously, mean wind was measured on ASIS with the cup anemometers at 1.18 m and 2.42 m, and with the sonic anemometers at 2.56 m and 5.3 m. The two measurements around 2.5 m agree very well in the mean for relative wind direction $|\delta\phi_r| < 30°$ (Fig. 7), but disagree otherwise. In the wind profile analysis only data with $|\delta\phi_r| < 30°$ will be used, i.e. the "profile data set". The 5-m mean wind measurements are not suitable for the profile analysis, as sonic measurements of mean wind have an uncertainty of significantly more than the ca. 1% required. The analysis in this sub-section is concentrated instead on the 1.18–2.42 m height interval.

The dimensionless wind gradient is defined as

$$\phi_m = \frac{kz}{u_*}\frac{\partial U}{\partial z} \qquad (6)$$

where k, as before, is von Karman's constant (≈ 0.40, *see* below). According to the classical Monin-Obukhov theory (Obukhov 1946), ϕ_m should be a function of only z/L in the constant flux layer. For $z/L = 0$, it is expected that $\phi_m = 1.0$. When ϕ_m values derived with Eq. 6 from the measurements at 1.18 and 2.42 m are plotted as a function of wave age, c_p/U_{10} (Fig. 12), data are seen to scatter around a mean value of 1.62, with no obvious trend. A similar result is found when ϕ_m is plotted against z/L and against U_{10} (not shown). Applying established formulas for $\phi_m(z/L)$ shows that expected individual values of ϕ_m

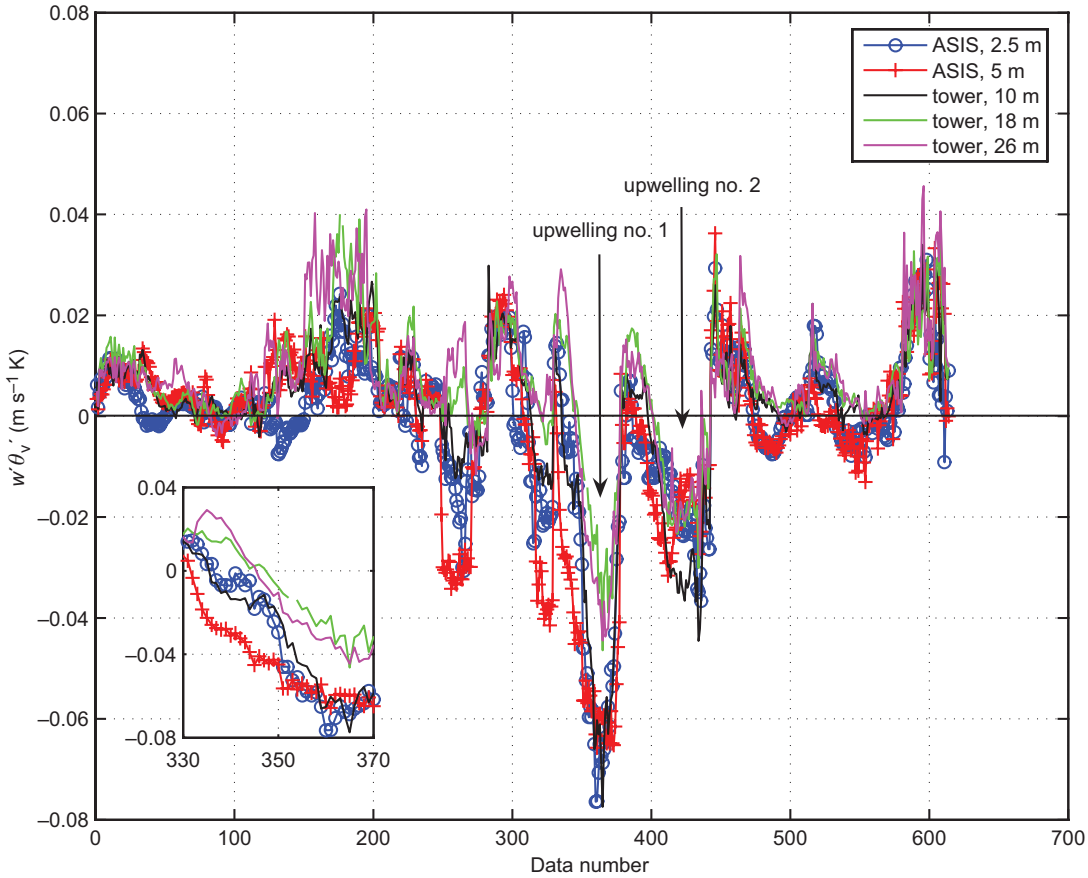

Fig. 11. Sensible heat flux (strictly speaking: virtual temperature flux) for two levels on ASIS and three levels on the tower against data number. Insert shows the situation during upwelling no. 1.

would be in the range 0.9–1.1 at this low height and with a mean value for the data set close to 1.0. The value of von Karman's constant (k) influences the value of ϕ_m in direct proportion. Thus, the value of $k = 0.25$ would be required to change the mean value of ϕ_m from 1.62 to 1.0. In the past, a wide range of k values have been suggested in atmospheric studies. But the work by Andreas *et al*. (2006) appears to have settled this question, with a value close to 0.40 now being accepted as very probably universally valid. Thus, another explanation for the observed high ϕ_m values must be found.

In conditions with high waves, a hypothetical possibility would be to introduce a zero plane displacement height (d) as done in studies of wind over high vegetation, etc. This can be tested by replacing z with $(z - d)$ in Eq. 6. By requiring $\phi_m = 1$, it is possible to derive d. The analysis (not shown) gives $d \approx$ constant = 0.6 m. This value is obtained irrespective of wind speed and significant wave height, which is physically unreasonable.

The 1.18-m anemometer is mounted on a 0.6-m-long boom attached to one of the 0.2-m-wide cylinders of the ASIS (Fig 2). This situation is likely to introduce a certain flow distortion at the site of the cups. Making first the simplified assumption that the circular cylinder is infinitely long, enables calculation of the potential flow caused by the cylinder (e.g. Milne-Thomson 1955). This gives a wind speed correction of about 1.5%, which is not enough to reduce ϕ_m from 1.62 to 1.0. In reality the local flow situation is more complicated, the cups being almost at the same level as the horizontal platform of ASIS (Fig. 2). Introducing a hypothetical corrected wind speed at 1.18 m, $U_{1.18m,\,cor} = aU_{1.18m,\,meas}$ that

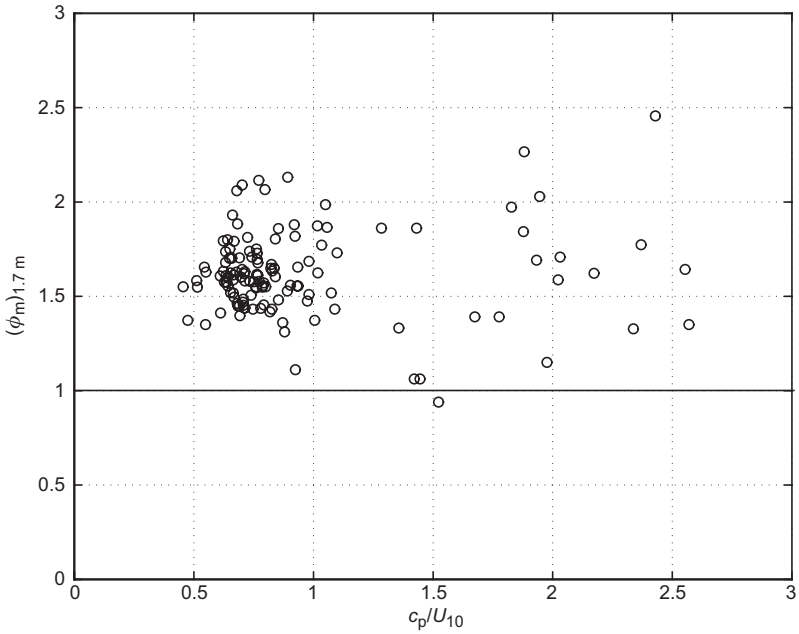

Fig. 12. ϕ_m derived from measured wind at 1.18 and 2.42 m on ASIS plotted against wave age c_p/U_{10}. Based on the "profile data set".

would give $\phi_m = 1.0$ for $k = 0.40$, enables determination of the factor a, the mean value of which is 1.045 with a standard deviation of 0.006. Plots of a against wind speed, wave age and stability (not shown) show no systematic trend. The data set consists of 142 values, so the standard error of the mean is 0.0005. It is reasonable to draw the conclusion that there is, in fact, a 4.5% flow distortion at the site of the 1.18 m cup anemometer. A plot (Fig. 13) of u_* at 2.56 m against

$$u_{*prof} = (U_{2.42m} - U_{1.18m,cor})/k^{-1}\ln(2.42/1.18),$$

with $k = 0.40$ shows good agreement with the theoretical log-law. The fit of the data is quite satisfactory. Thus, for further analysis which includes the 1.18 m level, a constant 4.5% correction is applied to all wind speed data from this level.

Dimensionless wind gradient functions

The dimensionless wind gradient ϕ_m (Eq. 6) has been evaluated for (1) stable conditions, i.e. $L > 0$ and (2) unstable, i.e. $L < 0$, with growing sea conditions, defined as $c_p/U_{10} < 0.8$. All analyses shown are based on the "profile data set".

For the stable case, mean wind was taken from 14.4 m and 30.1 m and u_* was obtained as a mean from all five turbulence levels (2.5, 5, 10, 18 and 26 m). ϕ_m plotted against z/L (Fig. 14) obtained from a regression line passing through [$x = 0$ and $y = 1$] gives:

$$\phi_m = 1 + 6.0z/L \qquad (7)$$

Linear profiles with large variations of the coefficient of the z/L term in stable conditions have been reported by many authors over the years. In a review article, Högström (1996) recommended the value 5.3 for the coefficient. A study from another Baltic Sea site (Bergström and Smedman 1995), which employed the very accurate MIUU turbulence instrument, gave 6.8 for the coefficient. Cheng and Brutsaert (2005) report 5.8 from their analysis of the extensive measurements during the CASES-99 experiment in Kansas. Note that the present experimental data are restricted to $z/L < 0.25$. According to Cheng and Brutsaert (2005), the linear range is expected to be restricted to $z/L < 0.8$.

Corresponding result for the unstable, growing sea case (Fig. 15) has been derived for two heights: 10.6 and 18.0 m. Also shown in that graph is a curve representing the expression obtained from several studies over land (e.g.

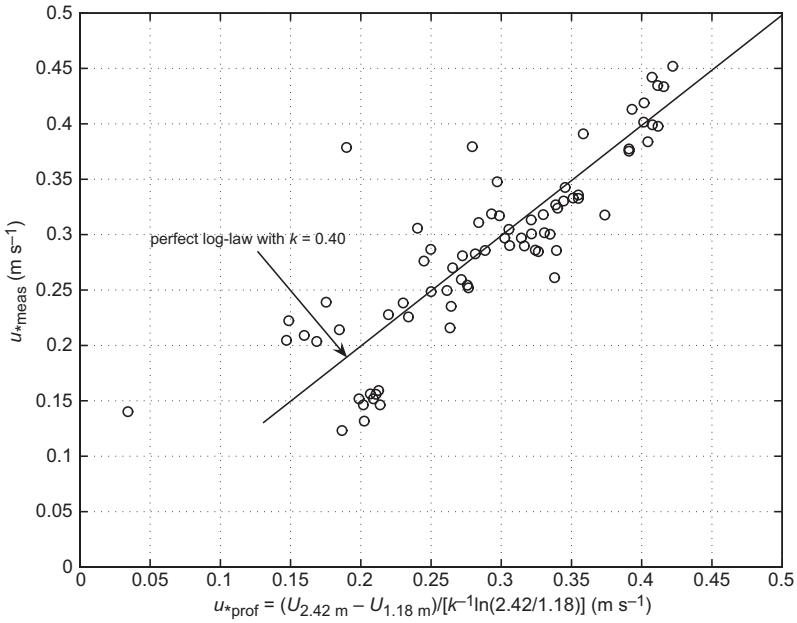

Fig. 13. Test that the wind profile in the layer 1.18 m to 2.42 m is logarithmic in the mean after 4.5% correction of the 1.18 m wind.

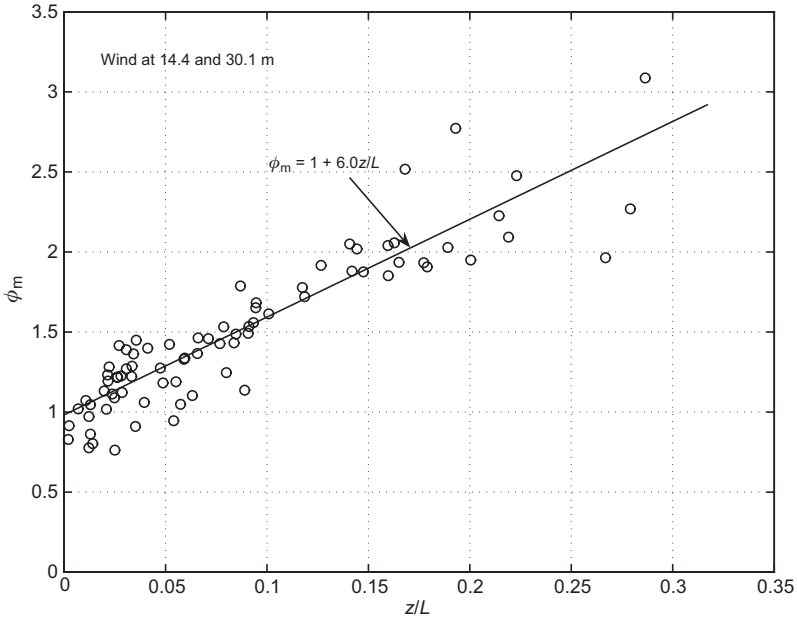

Fig. 14. ϕ_m for stable conditions, strictly valid at 22 m, derived from wind measurements at 14.4 and 30.1 m and mean u_* values from all three tower levels, plotted against z/L.

Högström 1996):

$$\phi_m = (1 - 19z/L)^{-1/4} \quad (8)$$

The data, although scattered, tend to be systematically below this curve. As discussed in detail later, this feature is interpreted as an effect of the height of the atmospheric boundary layer.

The trend of the bulk of the unstable data (Fig. 15) is most simply approximated by two straight lines which have the equations

$$\phi_m = 1 + 7.5z/L, 0 > z/L > -0.12 \quad (9)$$
$$\phi_m = 0.1, -0.12 > z/L > -1$$

Equations 7 and 9 will be used in next sub-

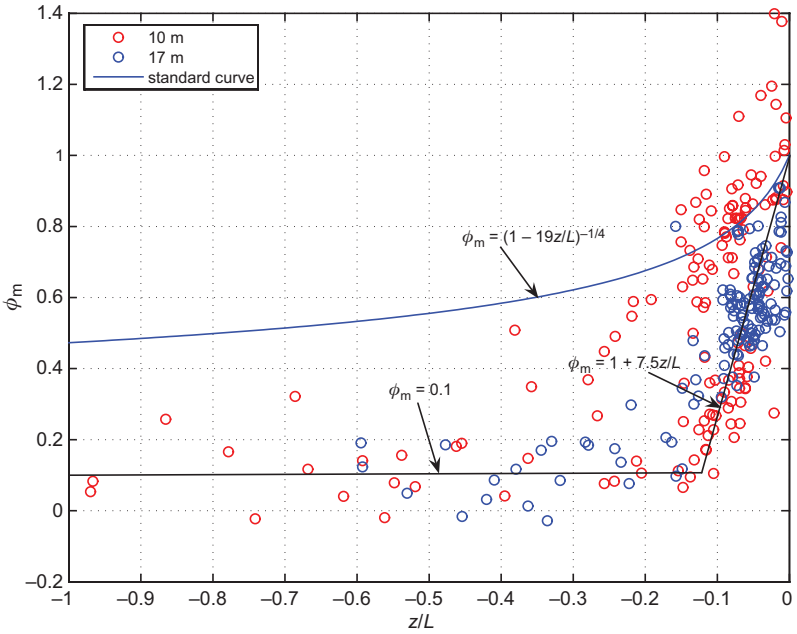

Fig. 15. ϕ_m for unstable, growing sea conditions, derived from tower data for 10.6 and 18.0 m, plotted against z/L. The curves are Eqs. 8 and 9, respectively.

section to derive mean wind profiles for stable and unstable conditions with growing sea for the entire 2.4–30 m layer.

Mean profiles for unstable and stable conditions

Provided u_* can be considered constant with height, Eq. 6 can be integrated from the surface or, more precisely, from $z = z_0$, where z_0 is the roughness length, to a height z to give:

$$U = \frac{u_*}{k}\left[\ln\left(z/z_0\right) - \psi_m\right] \quad (10)$$

where

$$\psi_m = \int_0^{z/L} \left\{\left[1 - \phi_m(\zeta)\right]/\zeta\right\} d\zeta \quad (11)$$

Provided the $\phi_m(z/L)$ functions (Eqs. 7 and 9) are valid throughout the entire layer studied, we will get profile functions which can be compared with measurements in this layer. Inserting Eq. 7 into Eq. 11 gives for the stable case:

$$\psi_m = -0.6z/L \quad (12)$$

An exactly similar expression is obtained for the unstable growing sea case for $-z/L < 0.12$ but with the constant 7.5.

From the "profile data set" one file for unstable, growing sea (N =143) has been extracted and another for stable (N = 178) conditions (denoted "stability groups" below for simplicity). Plotting the sea surface temperature measured at ASIS and at the two wave buoys (DWR4 and DWR5, cf. Fig. 1) for these two data sets (not shown) shows that for the unstable, growing sea case, the temperatures are very close: mean differences from any pairs of buoys being within ±0.05 K, having a standard deviation of about 0.25 K. For the stable data set, a very similar result is obtained for the first 100 data. The period $101 < N < 178$, however, is very different, with much larger mean differences and standard deviations, e.g. mean($T_{wASIS} - T_{wDR4}$) = 1.35 K, and the corresponding standard deviation is 1.43 K. This period is largely dominated by upwelling. In calculation of mean wind profile for stable conditions, only the first 100 data are used.

Mean wind speed has been derived for all "profile" levels (2.42 m, 8.0 m, 13.2 m, 15.6 m, 21.5 m and 30.1 m) for each of these two "stability groups" (Fig. 16).

To enable calculation with Eq. 10, mean values for the following parameters have been derived for the two 'stability groups': u_*, L and

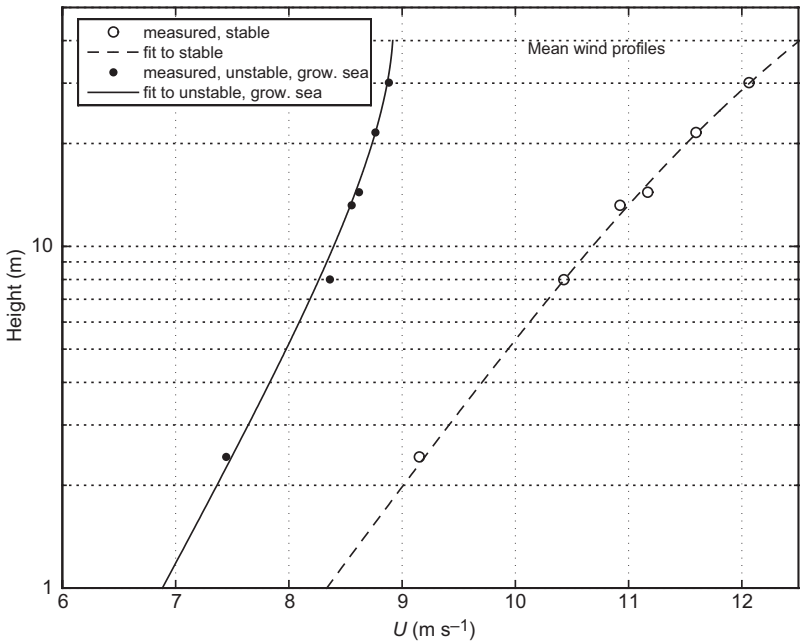

Fig. 16. Mean wind profiles in lin-log representation for unstable, growing sea (line and dots), and stable conditions (circles and dashed line). Circles are mean values measurements, and curves are fits to the profile equations (Eq. 10).

z_0. The latter is obtained from measurements of wind and u_* at 2.42 m, assuming a logarithmic wind profile below that height

$$z_0 = 2.42\exp(-kU_{2.42}/u_*) \qquad (13)$$

For the stable case, the following mean parameter values were derived: $u_* = 0.3812$ m s^{-1}; L = 337 m; $z_0 = 1.62 \times 10^{-4}$ m. Here, u_* and z_0 have been computed as ordinary means, but L has been derived from the mean of L^{-1}, as it is entered in this form into Eq. 12 and hence into Eq. 10 for U (dashed line in Fig. 16).

For the unstable, growing sea case, the corresponding mean values are: $u_* = 0.2875$ m s^{-1}; L = –342 m; $z_0 = 6.78 \times 10^{-5}$ m (solid line in Fig. 16). It is obvious that the respective profile fits come very close to the observed mean values. The mean values of the difference between measured and calculated wind are 0.01 m s^{-1} for the unstable, growing sea case and –0.04 m s^{-1} for the stable case; the corresponding standard deviations are 0.04 and 0.05 m s^{-1}, respectively. Thus, the 2.42-m wind speed fits the tower profile very well, with $\phi_m(z/L)$ functions deduced from the tower data. Note also that, as shown earlier, the profile between 1.18 m and 2.42 m is very close to logarithmic, which is in agreement with Eq. 10 when $|z/L|$ is so small that $\phi_m \approx 1$.

Matching of individual wind profiles

As demonstrated above, mean wind profiles constructed separately for all stable data and for all unstable, growing sea data from the 'profile' data set fit excellently from 2.42 m on ASIS to the top level (30 m) on the tower (Fig. 16). This is not the case when individual profiles are considered (which also include measurements from the 1.18-m level) for unstable, growing sea conditions (Fig. 17) and stable conditions (Fig. 18). In an attempt to reduce random scatter, each profile is the mean of data from 3–10 consecutive half-hour periods. Nevertheless, the mismatch of ASIS profiles extrapolated to 8 m and corresponding tower profiles is striking. Altogether ten unstable, growing sea profiles and twelve stable profiles were derived from the "profile data set", and all show the same general degree of random mismatch (for the sake of clarity of presentation, the number of profiles chosen for demonstration, in Figs. 17 and 18 were limited). Typically, the mismatch is of the order of 0.5 m s^{-1}. This may be interpreted as an effect of the instruments on ASIS and on the tower "seeing" different areas but it can also be the result of inherent turbulence dynamics, as discussed later. In any case, this is likely to be a random process.

If this is a correct assertion, it is expected

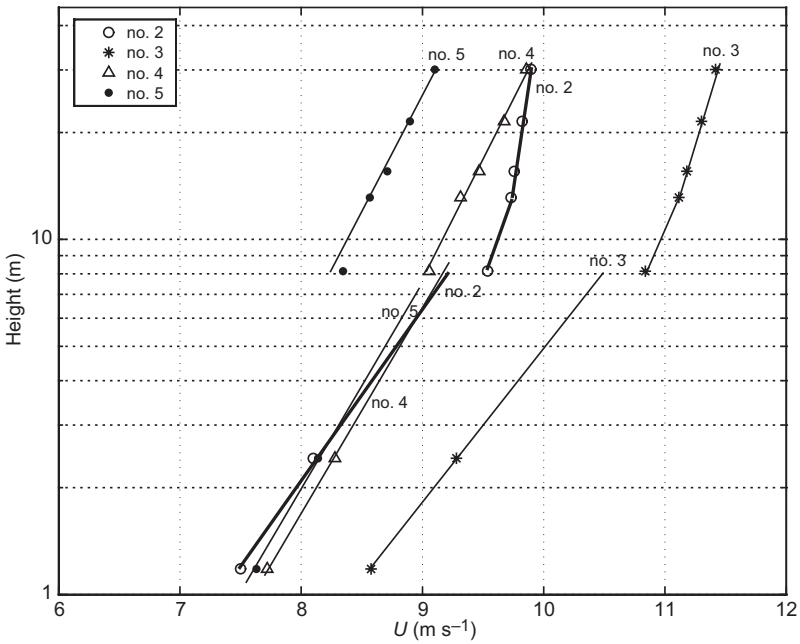

Fig. 17. Examples of individual wind profiles (each profile a mean over 1–5 hours) for unstable, growing sea conditions. Tentative fits have been added to each tower profile and each ASIS profile, extrapolated to 8 m. Profile numbers are included to facilitate identification of profile pairs. Profile no. 2 has been plotted with thick lines.

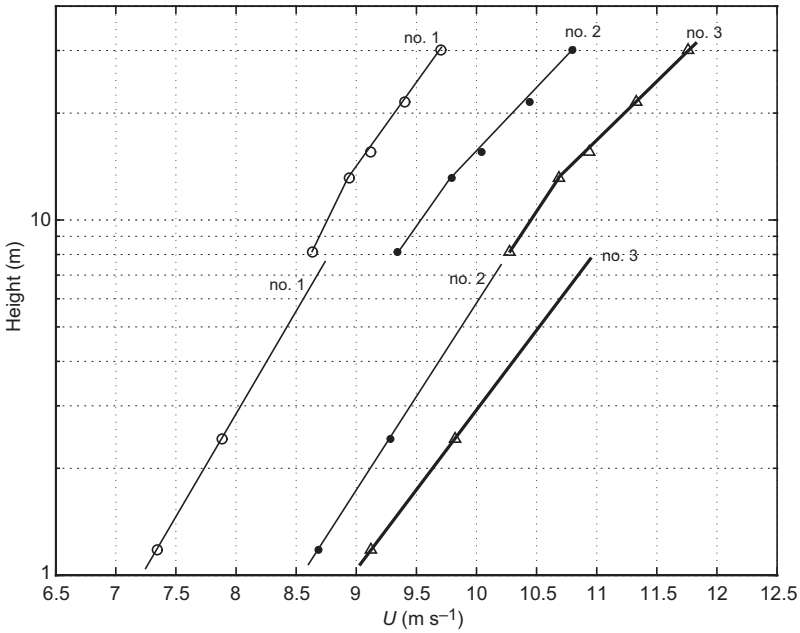

Fig. 18. As Fig. 17 but for stable conditions. Profile no. 3 has been plotted with thick lines.

that wind measurements at any two levels on the tower as well as at 1.18 m and 2.42 m on the ASIS are highly correlated, but that simultaneous measurements at one ASIS-level and one tower-level are much less well correlated. Thus (Table 4), for the pairs 1.18 and 2.42 m and 8.1 and 15.5 m, the mean residual variance (for unstable, growing sea and stable) is 0.005 m^2 s^{-2}, which strongly contrasts with the result for the pair 2.42 and 8.1 m, which is 0.224 m^2 s^{-2}. This corresponds to a site-dependent standard deviation of about 0.5 m s^{-1}, which is in order of magnitude agreement with the observed, apparently random, mismatch of measured tower profile data and extrapolated ASIS data at 8 m (Figs. 17 and 18). Notice that the data used for the profile

matching have been selected exclusively from measurements at one of the sites (Östergarnsholm, 8 m). With the data available also from ASIS, it might be argued that criteria of horizontal homogeneity of the wind field should also be enforced. But doing so would be to remove data which contain some of the information we are actually after. As discussed later, there are inherent characteristics in the wind field on a relatively large scale which are the likely causes of the observed random mismatch.

Roughness lengths and drag coefficients

From Eq. 10 the roughness length is obtained as:

$$z_0 = z\exp[-U(z)k/u_* - \psi_m] \qquad (14)$$

The "profile data set" for unstable conditions and growing sea has been used for evaluating z_0 in three different ways:

1. Mean wind U for z = 2.42 m: the effect of stability at this low height is considered negligible, so ψ_m is set to zero.
2. Mean wind for z = 10 m: ϕ_m is assumed to follow the standard formula (Eq. 8).
3. Mean wind for z = 10 m: ϕ_m is assumed to follow Eq. 9.

Mean z_0 for the entire data set (N = 750) is 1.28×10^{-4} m for the first case, 1.54×10^{-4} m for the second case and 1.24×10^{-4} m for the third case. These differences are small considering that the range of individual z_0 is from < 10^{-6} m to nearly 10^{-3} m. In general, the estimates made with the three methods follow each other closely (not shown). From this it is concluded that, for conditions with unstable air and growing sea, z_0 is surprisingly insensitive to the exact choice of stability function ϕ_m.

A plot of z_0/σ, with z_0 derived from measurements at 2.4 m (i.e. option 1 above) and σ is RMS surface elevation, against the wave age parameter u_*/c_p (not shown) shows general agreement with the previous results from Östergarnsholm (Smedman *et al*. 2003: fig. 9). The scatter of the data is considerable, but the trend is in general agreement with the following expression from Drennan *et al*. (2003), which was derived from several deep-sea measurement campaigns:

$$z_0/\sigma = 13.3(u_*/c_p)^{3.4} \qquad (15)$$

The drag coefficient is defined as:

$$C_D = [u_*/U(z)]^2 = k^2/[\ln(z/z_0) - \psi_m(z/L)]^2 \qquad (16)$$

Here ψ_m is derived with Eq. 11, which requires knowledge of the function $\phi_m(z/L)$. We want to evaluate the effect of the exact choice of $\phi_m(z/L)$ on the C_D/C_{DN} ratio, where the height z = 10 m and

$$C_{DN} = k^2/[\ln(10/z_0)]^2 \qquad (17)$$

is the expression obtained from Eq. 16 at neutral conditions, for which $\psi_m = 0$. We make the evaluation for the unstable, growing sea case, using (i) the 'standard' Eq. 8 and (ii) our new Eq. 9 (Table 5). The new formulation gives C_D/C_{DN} ratios larger than the "standard" formulation; the difference increasing with $-z/L$: for $-z/L < 0.1$ the two formulations differ by less than 10%, for

Table 4. Correlation analysis of wind at two levels. The table gives the residual variance of measured wind speed relative to linear regression for measurements at three pair of heights ($m^2\ s^{-2}$).

Heights (m)	Unstable conditions (growing sea)	Stable conditions
1.18 and 2.42	0.006	0.001
2.42 and 8.1	0.176	0.272
8.1 and 15.5	0.008	0.006

Table 5. Variation of the drag coefficient ratio C_D/C_{DN} with stability at the 10-m height for the unstable (growing sea) case for two alternative ϕ_m formulations: the "standard" formulation (Eq. 8), and the expression fitted to the observations in Fig. 19 (Eq. 9).

$10/L$	$(C_D/C_{DN})_{standard}$	$(C_D/C_{DN})_{Eq.\ 9}$
–0.05	1.03	1.07
–0.1	1.05	1.15
–0.2	1.08	1.29
–0.3	1.11	1.39
–0.7	1.18	1.65
–1.0	1.22	1.78

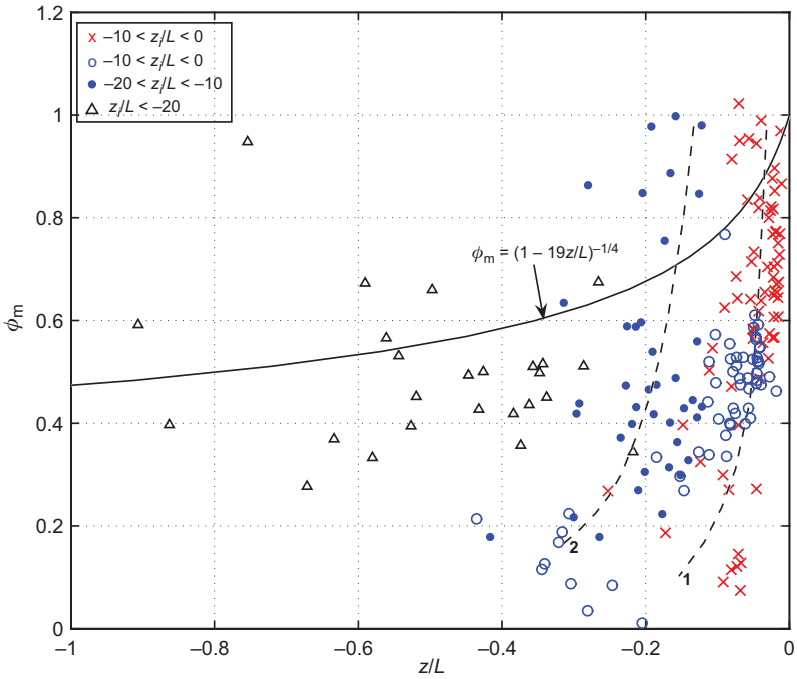

Fig. 19. ϕ_m for unstable conditions, derived from Östergarnsholm tower data from the present experiment (filled blue circles), and from the previous data set (Johansson *et al.* 2003) (remaining symbols) plotted against z/L. Dashed lines 1 and 2 are tentative data fits representing z_i/L = –5 and z_i/L = –15, respectively.

z/L = –0.2 the difference is about 19% and for z/L = –0.7 the new ratio is 46% larger than the ratio derived with the standard formulation.

Discussion

Two particular results from the last section will be discussed: (i) the failure of the ϕ_m data for unstable, growing sea conditions (Fig. 15), to adhere to the expected 'standard curve' (Eq. 8), and (ii) the mismatch of individual tower and ASIS wind profiles (Figs. 17 and 18).

$\phi_m(z/L)$ relations for unstable situations

The present data for unstable, growing sea conditions (Fig. 15) are not only scattered but tend to deviate strongly towards the low side of the expected 'standard curve' (Eq. 8). In the corresponding plot (Fig. 19) of data based on a much larger data set from Östergarnsholm (Johansson *et al.* 2003) together with the data from the present study, the data were stratified according to the magnitude of z_i/L, where z_i is the depth of the unstable boundary layer. Data having –10 < z_i/L < 0 have very much the same trend as the present data (Fig. 15), whereas data with z_i/L < –20 scatter around the curve described by Eq. 8. Thus, it would be appropriate to ask what boundary layer heights prevailed during BASE?

Twelve radio soundings were made at Östergarnsholm during 6–10 September 2003 and eight from r/v *Aranda* stationed close to Östergarnsholm during 5–11 September. The height of the boundary layer, z_i was evaluated from the radio soundings as the height to the first inversion and was found to range between 50 m and 240 m in the first 11 soundings, which cover the period 5–9 September, rose to between 330 and 450 m on 10 September and dropped again to 200–300 m on 11 September. The observed individual z_i values were plotted as a function of time, and it was found that the estimates from the two data sets agree very well (not shown). Heights were interpolated so that z_i/L could be derived for each half hour. The result is that –10 < z_i/L < 0 for each of the growing sea cases during this particular period (filled blue circles in Fig. 19). Although 5–11 September 2003 corresponds to only about 20% of the total BASE period used here, it is worth noting that in the rather extensive data set that makes up this plot,

the cases with $-10 < z_i/L < 0$ constitute a large proportion of the total number of cases. It is thus not unreasonable to attribute the strong descending branch of data observed to the effect of the limited boundary layer height. Note, that in the data from the present experiment (Fig. 15) there are some which appear to adhere to Eq. 8 and which may have larger $-z_i/L$ values.

An influence of the boundary layer height on surface layer scaling was first discovered by Khanna and Brasseur (1997) in their high-resolution large-eddy simulations (LES) of the convective atmospheric boundary layer. These model results were successfully tested against a set of atmospheric data, including extensive radio soundings (Johansson *et al*. 2001), which enabled determination of the height of the boundary layer z_i, a quantity which is lacking in most surface-layer experiments.

In a follow-up study, Johansson *et al*. (2003) derived boundary layer height either (i) directly, from numerous radio soundings at Östergarnsholm or (ii) from simulations with an internal convective boundary layer model (Gryning and Batchvarova 2002), the performance of which was first validated against a set of radio soundings at Östergarnsholm. The data (Fig. 19) show a clear division of ϕ_m according to z_i/L, in agreement with the findings in the LES of Khanna and Brasseur (1997) and the previous atmospheric study by Johansson *et al*. (2001). Note the very good agreement of the data from the present study (filled blue circles) with the corresponding data from the Johansson *et al*. (2001) study for the same z_i/L range (red crosses).

In the previous section it was shown that the shape of the ϕ_m function in unstable conditions has a considerable importance in converting from C_{DN} to C_D, as done in most large-scale atmospheric models. This illustrates that it is important to learn more about the basic mechanism that creates this deviation from "classical" behaviour, as well as about climatological incidence of relatively low boundary layer height and large negative L values in different marine environments. If such study shows that conditions with small negative z_i/L values occur for appreciable times and over appreciable areas, the ability of present day large-scale models to resolve the boundary layer height must be assessed.

The mismatch of individual tower and ASIS wind profiles

In order to understand the observed profile mismatch (Figs. 17 and 18), spectral analysis has been carried out on part of the data which was used in the previous analysis. Three unstable, growing sea cases and two stable cases, each consisting of 1.5 to 5 consecutive hours of data, were selected for the analysis, and the following spectral estimates were derived: (i) longitudinal wind component spectra, $nS_u(n)$, at 5 m on ASIS and at 10 and 26 m on the tower, where n is frequency (Hz); (ii) vertical velocity spectra for the same heights, $nS_w(n)$; (iii) co-spectra and quadrature spectra based on the longitudinal wind data from ASIS 5 m and the tower, 10 m, $Co_{u5m,u10m}(n)$ and $Q_{u5m,u10m}(n)$ respectively; (iv) coherence of the longitudinal wind component at 5 and 10 m, defined as

$$\mathrm{Coh}(n) = \frac{\mathrm{Co}^2_{u5m,u10m}(n) + Q^2_{u5m,10m(n)}(n)}{nS_{u5m}(n)\,nS_{u10m}(n)} \quad (18)$$

Sometimes the square root of this expression is called the coherence, but here we prefer Eq. 18, as it gives the spectral energy that is correlated at the two measuring points.

Figure 20 shows, for one typical case (stable conditions; U_{10} = 12.4 m s^{-1}), the coherence (upper graph) and the corresponding longitudinal spectra (lower graph). It is notable that the coherence is virtually zero for $n > 2 \times 10^{-3}$ Hz and unity for $n < 2 \times 10^{-4}$ Hz. This means that for $n > 2 \times 10^{-3}$ Hz, the fluctuations in u are completely uncorrelated and that for $n < 2 \times 10^{-4}$ Hz, they are completely correlated. The frequency where $\mathrm{Coh}(n) = 0.5$ is about 4×10^{-4} Hz. Assuming Taylor's hypothesis for "frozen turbulence" is valid — which cannot be taken for granted at these frequencies, but which is experimentally supported by the study of Högström *et al*. (1999) — we obtained corresponding, but very approximate atmospheric wave lengths, $\lambda = U/n$: for $\mathrm{Coh}(n) = 0$, $\lambda = 6$ km; $\mathrm{Coh}(n) = 0.5$, $\lambda = 30$ km; $\mathrm{Coh}(n) = 1.0$, $\lambda = 60$ km. The analysis shows that these values are representative of the five cases studied, with no systematic difference between the slightly stable and the slightly unstable cases — the u spectra are, for this particular purpose, very similar (cf. Högström *et al*. 2002). This

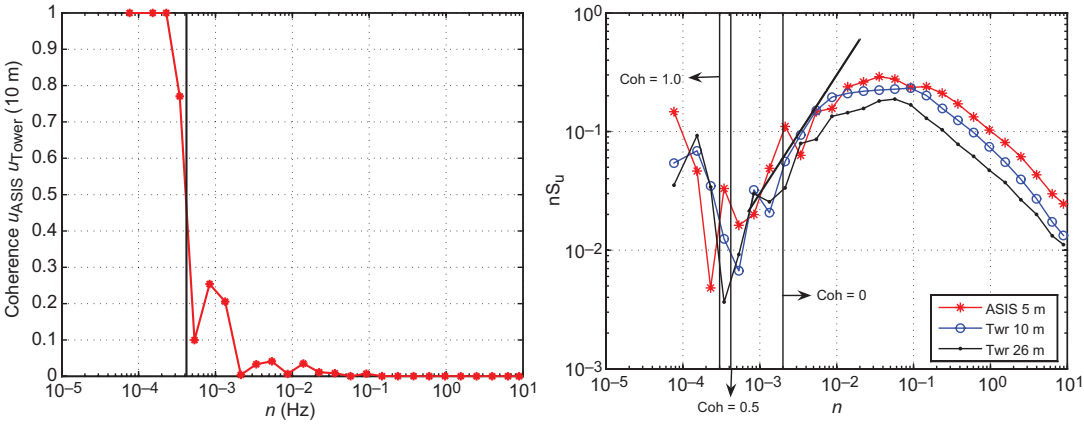

Fig. 20. Example of coherence between wind at 10 m on the tower and 5 m on ASIS (left-hand side panel) and longitudinal wind spectra from ASIS, 5 m, and the tower, 10 and 26 m (right-hand side panel).

would explain the observed uncorrelated wind variance (about 0.25 m^2 s^{-2}).

It is pertinent to ask about the nature of the fluctuations in the approximate frequency domain 2×10^{-4} Hz $< n < 2 \times 10^{-3}$. Comparison of the u spectra (Fig. 20) with the corresponding vertical velocity spectra (not shown) reveals that the w-spectral energy is about 100 times lower than the corresponding u spectral energy in this frequency range, so that the corresponding structures must be quasi-two-dimensional. This result is obtained for all the five studied cases.

The right-hand side panel of Fig. 20 shows that longitudinal spectra from the three heights 5, 10 and 26 m tend to collapse in the approximate frequency range 10^{-3} Hz $< n < 5 \times 10^{-3}$ Hz, with a slope of 1.0, i.e. $nS_u(n) \propto n$. The tangent line drawn in the $nS_u(n)$ plot (Fig. 20) has this slope, which is in agreement with predictions for neutral turbulent boundary-layer flow (Perry *et al*. 1986, Hunt and Morrison 2000). Note that for $n > 10^{-2}$ Hz the spectra do not collapse in this representation, in agreement with predictions from surface layer scaling, they instead collapse when spectra are plotted against nz/U (not shown). For $n > 3 \times 10^{-1}$ Hz, $nS_u(n) \propto n^{-2/3}$ approximately, as predicted for the inertial subrange.

As discussed by Högström *et al*. (2002), then $nS_u(n) \propto n$ regime is a manifestation of "very large-scale structures" of the atmospheric surface layer, probably identical to longitudinal streaks found in the logarithmic layer. They appear to be "dynamically 'preferred modes' of neutral boundary-layer flow". These "longitudinal streaks" have been observed in large-eddy simulations of the neutral boundary layer (Foster and Dobrinski 2000), and in high-Reynolds number laboratory flows by Kim and Adrian (1999) and others and have the form of long "band-like" structures. Note that this spectral range in the u spectra (Fig. 20) ends rather abruptly at a frequency near the point where Coh = 0.5 and turns into a rapid spectral energy increase with decreasing frequency. As discussed by Högström *et al*. (1999) and observed in studies in the free troposphere and lower stratosphere (Nastrom *et al*. 1985), this is the beginning of a wide spectral range which extends several decades in descending frequency, with $nS_u(n) \propto n^{-2/3}$. This is a manifestation of "pancake-like" motions, which are very likely quasi-two-dimensional turbulence (*see* Nastrom *et al*. 1985, Högström *et al*. 1999). Note, that the spectral energy cascade in this range is up-scale (not down-scale as in the well-known inertial sub-range which, accidentally, happens to have the same $nS_u(n) \propto n^{-2/3}$ form).

An interesting consequence of this analysis is that most of the proper turbulent energy measured simultaneously on ASIS and on the tower is strictly speaking statistically uncorrelated, i.e. having a coherence close to zero. Hence our finding above that the momentum fluxes measured simultaneously at ASIS and the tower agree so well means that the turbulence field is horizontally very homogenous in the mean for most cases studied here (except for the upwelling

cases), and that the placement of the tower on a piece of land does not in any measurable way deteriorate the measurements.

That this result has nothing to do with particular marine or coastal conditions is illustrated in the Appendix for a case with measurements in homogeneous land conditions. A high instrumented tower was placed only 50 m from an instrumented mast. As a mean over 228 hours of simultaneous measurements, the difference of wind speed measured at 9 m on the tower and on the mast was only 0.013 m s^{-1}. In striking contrast, the standard deviation of the difference for hourly means was as high as 0.34 m s^{-1}, a result which is likely to have the same general explanation as the phenomenon observed in the present study.

Conclusions

The momentum flux measured at 10 m on the Östergarnsholm tower agrees very well in the mean with the corresponding flux measured on ASIS. No directional effect due to possible wave field heterogeneity is found for winds from 80°–210°. The homogeneity of the momentum flux field was also evident in the horizontal measurement tracks made with r/v *Aranda*. The flux of sensible heat appears to behave similarly to the momentum flux, but the scatter in the comparisons is much larger, which was expected, since the signal to noise ratio is often low for the sensible heat flux measured with the R2/R2A sonic anemometers.

Extrapolated wind profiles based on measurements on the tower and on ASIS do not fit on an individual basis when wind is averaged over one to several hours. In the mean the profiles do, however, fit. What is said here about good profile fit in the mean appears to be true for most conditions encountered during BASE, with the exception of two periods (each roughly a day long) characterized by pronounced upwelling, when strong heterogeneity in sea surface temperature was observed.

Analysis of dimensionless profile function $\phi_m(z/L)$ has been performed on the data from the tower for two characteristic situations: (i) stable conditions and (ii) unstable conditions with growing sea. For the stable case it was found that $\phi_m(z/L)$ increases linearly with z/L with a slope factor that is in fair agreement with other studies.

For the unstable, growing sea case it is found that $\phi_m(z/L)$ is much below predictions from generally accepted formulations for most cases. It is concluded that this feature is due to an indirect influence of the boundary layer depth on ϕ_m, being particularly strong when the boundary layer height is low and the Obukhov length $-L$ large, which was the case during at least a period of a week with 20 radio soundings, which enabled determination of the boundary layer height.

The roughness length z_0 was derived for the unstable, growing sea case and was found to be insensitive to the exact choice of the function for $\phi_m(z/L)$ and to a have wave-age dependence in general agreement with what was found over the deep sea. The transformation from neutral drag coefficient C_{DN} to C_D, however, includes integration of $\phi_m(z/L)$ from the surface of the ocean to 10 m. It was shown that what we interpret as an effect of the boundary layer height, has a considerable impact on C_D — of the order 10%–50% in the stability interval $-0.1 > z/L > -0.7$.

Thus, in most cases, with winds from 80–210°, the measurements on the Östergarnsholm tower do indeed represent upwind open sea conditions. This is true in a statistical mean sense. But, as a result of random fluctuations on a horizontal scale of order 5–50 kilometers, profiles of wind (and most likely temperature) measured during a particular hour are unlikely to correspond exactly with simultaneous profiles in areas a few kilometres upwind. During situations when upwelling occurs, the boundary conditions (especially sea surface temperature) are strongly heterogeneous on a relatively small scale that may temporarily invalidate the above general conclusion. It should be noted also that there is a high wind bias in the data set used in this analysis. The conclusions may not hold for light wind conditions, in particular perhaps in situations dominated by swell, which will be the subject of forthcoming papers based on analysis of BASE data.

Acknowledgements: Participation of the Uppsala group was made possible by funding by The Swedish Research Coun-

cil, grant no. 621-2002-5348. We thank Dr. Hans Bergström and other colleagues at MIUU who are responsible for the measurements at Östergarnsholm. We thank the following for various aspects of this work on land and sea: Joe Gabriele, Mike Rebozo, Henry Söderman, Teuvo Seppälä, Jari Helminen, Hannu Jokinen and Elina Miettunen as well as the captain and crew of the r/v *Aranda*. WD and FZ acknowledge support from the National Science Foundation, grant OCE-0220459.

References

Andreas E.L., Claffey K.J., Jordan R.E., Fairall C.W., Guest P.S., Persson P.O.G. & Grachev A.A. 2006. Evaluations of the von Kármán constant in the atmospheric surface layer. *J. Fluid Mech*. 559: 117–149.

Bergström H., Johansson P.-E. & Smedman A. 1988. A study of wind speed modification and internal boundary-layer heights in a coastal region. *Boundary-Layer Meteorol*. 42: 313–335.

Bergström H. & Smedman A. 1995. Stably stratified flow in a marine atmospheric surface layer. *Boundary-Layer Meteorol*. 72: 239–265.

Cheng Y. & Brutsaert W. 2005. Flux-profile relationships for wind speed and temperature in the stable atmospheric boundary layer. *Boundary-Layer Meteorol*. 114: 519–538.

DeCosmo J., Katsaros K.B., Smith S.D., Anderson R.J., Oost W.A., Bumke K. & Chadwick, H. 1996. Air–sea exchange of water vapor and sensible heat: the humidity exchange over the sea (HEXOS) results. *J. Geophys. Res*. 101: 12001–12016.

Donelan M.A., Hamilton J. & Hui W.H. 1985. Directional spectra of wind generated waves. *Phil. Trans. R. Soc. London A* 315: 509–562.

Drennan W.M., Donelan M.A., Madsen N., Katsaros K.B., Terray E.A. & Flagg C.N. 1994. Directional wave spectra from a Swath ship at sea. *J. Atmos. Oceanic Tech*. 11: 1109–1116.

Drennan W.M., Graber H.C., Hauser D. & Quentin C. 2003. On the wave age dependence of wind stress over pure wind seas. *J. Geophys. Res*. 108, 8062, doi:1029/2000JC000715.

Foster R.C. & Drobinski P. 2000. Near-surface streaks: comparison of LES with theory. In: *Proceedings of the 14th Symposium on Boundary Layers and Turbulence, Aspen, CO, 7–11 August 2000*, American Meteorol. Soc., Boston MA, pp. 499–502.

Gerling T.W. 1992. Partitioning sequences and arrays of directional ocean wave spectra into component wave systems. *J. Atmos. Oceanic Technol*. 9: 444–458.

Graber H.C., Terray E.A., Donelan M.A., Drennan W.M., Van Leer J.C. & Peters D.B. 2000. ASIS — a new air–sea interaction spar buoy: design and performance at sea. *J. Atmos. Oceanic Technol*. 17: 708–720.

Gryning S.-E. & Batchvarova E. 2002. Marine boundary layer and turbulent flux over the Baltic Sea: measurements and modelling. *Boundary-Layer Meteorol*. 103: 29–47.

Hristov T.S., Miller S.D. & Friehe C.A. 2003. Dynamical coupling of wind and ocean waves through wave-induced air flow. *Nature* 422: 55–58.

Hunt J.C.R. & Morrison J.F. 2000. Eddy structure in turbulent boundary layers. *Euro J. Mech, B — Fluids* 19: 673–694.

Högström, U. 1996. Review of some basic characteristics of the atmospheric surface layer. *Boundary-Layer Meteorol*. 78: 215–246.

Högström U. Smedman A. & Bergström H. 1999. A case study of two-dimensional stratified turbulence. *J. Atmos. Sci*. 56: 959–976.

Högström U., Hunt J.C.R. & Smedman A. 2002. Theory and measurements for turbulence spectra and variances in the atmospheric neutral surface layer. *Boundary-Layer Meteorol*. 103: 101–124.

Johansson C., Smedman A.-S., Högström U., Brasseur J.G. & Khanna S. 2001. Critical test of the validity of Monin-Obukhov similarity during convective conditions. *J. Atmos. Sci*. 58: 1549–1566.

Johansson C., Smedman A.-S., Bergström H. & Gryning S.-E. 2003. *Influence of boundary layer height on turbulence structure in the marine atmospheric surface layer over the Baltic Sea*. Acta Universitas Upsaliensis, Comprehensive Summaries of Uppsala dissertations from the faculty of Science and Technology 792.

Kaimal J.C. & Gaynor J.E. 1991: Another look at sonic anemometry. *Boundary-Layer Meteorol*. 56: 401–410.

Khanna S. & Brasseur J.G. 1997. Analysis of Monin-Obukhov similarity from large-eddy simulation. *J. Fluid Mech*. 345: 251–286.

Kim K.C. & Adrian R.J. 1999. Very large-scale motion in the outer layer. *Physics of Fluids* 11: 417–422.

Komen G.J., Cavaleri L., Donelan M., Hasselmann, K., Hasselmann, S. & Janssen, P.A.E.M. 1994. *Dynamics and modelling of ocean waves*. Cambridge University Press.

Milne-Thomson L.M. 1955. *Theoretical hydrodynamics*, 3rd ed. Macmillan & Co. Ltd., London.

Nastrom G.D. & Gage K.S. 1985. A climatology of atmospheric wavenumber spectra of wind and temperature observed by commercial aircraft. *J. Atmos. Sci*. 42: 950–960.

Obukhov A.M. 1946. Turbulence in a thermally inhomogeneous atmosphere. *Trudy In-ta Teor. Geofiz. AN SSSR* 1: 95–15. [English translation in *Boundary-Layer Meteorol*. 2: 7–29].

Oost W.A. 1998. The KNMI HEXMAX stress data: a reanalysis. *Bound.-Layer Meteorol*. 86: 447–468.

Pasquill F. & Smith F.B. 1983. *Atmospheric diffusion*, 3rd ed. Ellis Horwood Ltd., Chichester.

Perry A.E., Henbest S. & Chong M.S. 1986. A theoretical and experimental study of wall turbulence. *J. Fluid Mech*. 165: 163–199.

Pettersson H., Graber H.C., Hauser D., Quentin C., Kahma K.K., Drennan W.M. & Donelan M.A. 2003. Directional wave measurements from three wave sensors during the FETCH experiment. *J. Geophys. Res*. 108(C3), 8061, doi:10.1029/2001JC001164.

Schmitt K.F., Friehe C.A. & Gibson C.H. 1979. Structure

of marine surface layer turbulence. *J. Atmos. Sci.* 36: 602–618.

Smedman A., Högström U. & Bergström H. 1997. The turbulence regime of a very stable marine airflow with quasi-frictional decoupling. *J. Geophys. Res.* 102: 21049–21059.

Smedman A., Högström U., Bergström H., Rutgersson A., Kahma K.K. & Pettersson H. 1999. A case-study of air-sea interaction during swell conditions. *J. Geophys. Res.* 104: 25833–25851.

Smedman A., Guo-Larsén X., Högström U., Kahma K.K. & Pettersson H. 2003. The effect of sea state on the momentum exchange over the sea during neutral conditions. *J. Geophys. Res.* 108(C11), 3367, doi: 10.1029/2002JC001526.

Smedman A., Högström U., Sahlee E. & Johansson C. 2007. Critical re-evaluation of the bulk transfer coefficient for heat over the ocean. *Quart. J. Roy. Meteorol. Soc.* 133: 227–250.

Smith S.D. 1980. Wind stress and heat flux over the ocean in gale force winds. *J. Phys. Ocean.* 10: 709–726.

Stull R.B. 1988. *An introduction to boundary layer meteorology*. Kluwer Academic Publ., Dordrecht/Boston/London.

Appendix

Wind inter-comparison at a homogeneous land site

In a wind energy-related project, wind speed was measured at several levels on a 145-m tower situated on a flat heath with scattered juniper bushes. The lowest level was 9 m, and in order to get an estimate of the wind profile at lower heights, during a special study it was decided to erect a 15-m mast only 50 m away from the main tower. The mast was equipped with cup anemometers at four levels from 2 m to 12 m. Figure A1 shows the mean wind profile measured simultaneously on the high tower and on the 15 m mast during a period of 228 hours. It is seen that the two profiles match very well. The mean difference at the overlapping height of 9 m is only 0.013 m s^{-1}. The standard deviation of the difference in hourly mean winds at this height is, however, as high as 0.34 m s^{-1}. Figure A2 shows some typical examples of individual simultaneous one hour mean profiles. The mismatch displayed in these profiles is similar to what is displayed in the present study (Figs. 17 and 18).

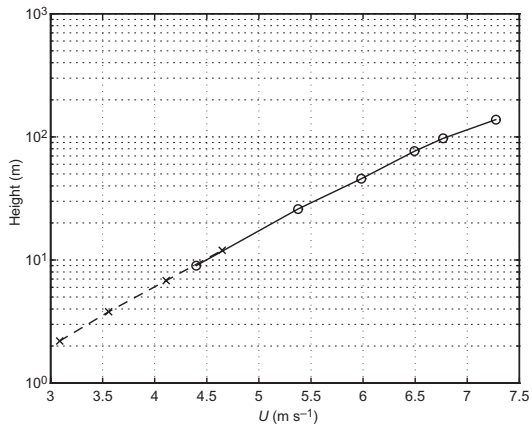

Fig. A1. Mean wind profile from Näsudden, based on 228 hours of simultaneous measurements on a 145 m tower (o) and on a 15 m mast (x) situated 50 m from each other.

These measurements were conducted on the Näsudden peninsula situated on the south-west coast of Gotland (cf. map in Bergström *et al.* 1988). The 145-m tower and 15-m mast were both placed centrally on the peninsula, with water (the Baltic Sea) at about 1500-m distance throughout the sector of dominating winds, from 50° over south to 320°. As mentioned above, the area is flat heath with uniform vegetation. As seen from the footprint analysis (Table 1), more than 80% of the flux measured at 10 m is expected to come from distances < 1500 m in neutral and unstable conditions. Thus effects from the terrain discontinuity at the coast line are likely to be marginal.

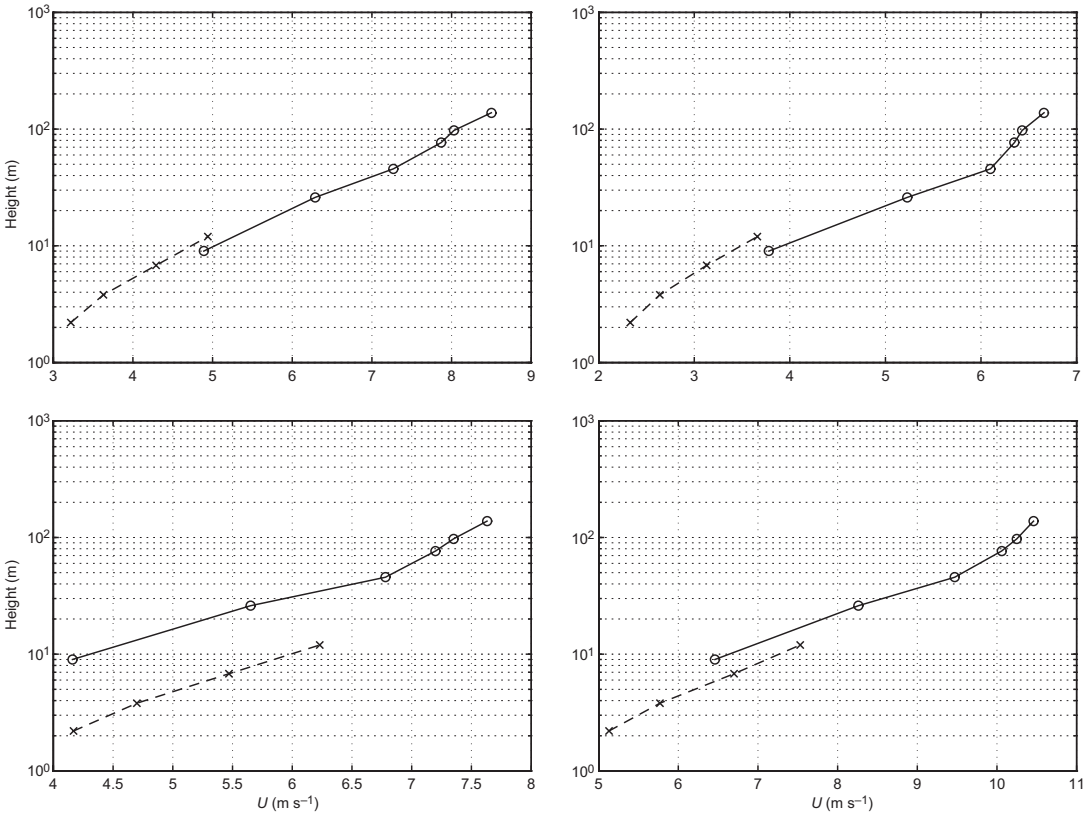

Fig. A2. Examples of individual hourly mean profiles from Näsudden.